DAHLGREN DIVISION
NAVAL SURFACE WARFARE CENTER
Dahlgren, Virginia 22448-5100

NSWCDD/TR-99/98

EXPECTED IMPROVEMENT IN NIMA PRECISE ORBIT AND CLOCK ESTIMATES DUE TO ADDING CROSSLINK RANGING DATA

BY MICHAEL J. MERRIGAN AND EVERETT R. SWIFT

THEATER WARFARE SYSTEMS DEPARTMENT

AUGUST 1999

Report Documentation Page

Form Approved
OMB No. 0704-0188

1. REPORT DATE	2. REPORT TYPE	3. DATES COVERED
AUG 1999		**00-00-1999 to 00-00-1999**

4. TITLE AND SUBTITLE	5a. CONTRACT NUMBER
Expected Improvement in NIMA Precise Orbit and Clock Estimates Due to Adding Crosslink Ranging Data	5b. GRANT NUMBER
	5c. PROGRAM ELEMENT NUMBER
6. AUTHOR(S)	5d. PROJECT NUMBER
	5e. TASK NUMBER
	5f. WORK UNIT NUMBER
7. PERFORMING ORGANIZATION NAME(S) AND ADDRESS(ES) **Dahlgren Division,Naval Surface Warfare Center,Dahlgren,VA,22448-5100**	8. PERFORMING ORGANIZATION REPORT NUMBER
9. SPONSORING/MONITORING AGENCY NAME(S) AND ADDRESS(ES)	10. SPONSOR/MONITOR'S ACRONYM(S)
	11. SPONSOR/MONITOR'S REPORT NUMBER(S)

12. DISTRIBUTION/AVAILABILITY STATEMENT
Approved for public release; distribution unlimited

13. SUPPLEMENTARY NOTES

14. ABSTRACT

15. SUBJECT TERMS

16. SECURITY CLASSIFICATION OF:			17. LIMITATION OF ABSTRACT	18. NUMBER OF PAGES	19a. NAME OF RESPONSIBLE PERSON
a. REPORT **unclassified**	b. ABSTRACT **unclassified**	c. THIS PAGE **unclassified**	**Same as Report (SAR)**	**44**	

REPORT DOCUMENTATION PAGE

Form Approved
OMB No. 0704-0188

1. AGENCY USE ONLY (Leave blank)	2. REPORT DATE	3. REPORT TYPE AND DATES COVERED
	August 1999	Final

4. TITLE AND SUBTITLE

Expected Improvement in NIMA Precise Orbit and Clock Estimates Due to Adding Crosslink Ranging Data

5. FUNDING NUMBERS

6. AUTHOR(s)

Michael Merrigan and Everett R. Swift

7. PERFORMING ORGANIZATION NAME(S) AND ADDRESS(ES)

Commander
Naval Surface Warfare Center
Dahlgren Division (Code T12)
17320 Dahlgren Road
Dahlgren, VA 22448-5100

8. PERFORMING ORGANIZATION REPORT NUMBER

NSWCDD/TR-99/98

9. SPONSORING/MONITORING AGENCY NAME(S) AND ADDRESS(ES)

10. SPONSORING/MONITORING AGENCY REPORT NUMBER

11. SUPPLEMENTARY NOTES

12a. DISTRIBUTION/AVAILABILITY STATEMENT

Approved for public release; distribution is unlimited.

12b. DISTRIBUTION CODE

13. ABSTRACT (Maximum 200 words)

With the deployment of GPS Block IIR and IIF satellites, crosslink data will be collected and used on-board for navigation. This motivated an effort to investigate the expected orbit and clock accuracy if crosslink data are available for post-processing on the ground. This study addresses the expected improvement in the National Imagery and Mapping Agency (NIMA) precise orbit and clock estimates with the inclusion of crosslink ranging data with the station tracking data. Simulated station data were created to reflect orbit and clock accuracy associated with NIMA production. Station tracking data were simulated for both 12- and 18-station networks covering 5 days to allow for three overlapping 3-day fit spans, with the middle day of each fit span used for analysis. Simulated crosslink ranging data, including pseudorange data, derived distance data, and derived clock data, were generated for the same 5 days and merged with the station data. Initially, a study was conducted to determine what satellite-related clock and crosslink bias parameters can be estimated with crosslink data types by themselves or in combination with station tracking data. Experiments were then conducted to investigate the characteristics and relative information content of the crosslink data types, including appropriate treatment and statistical assumptions for the crosslink biases. The sensitivity of precise orbit and clock estimates to various processing scenarios was also evaluated. Finally, the overall achievable orbit and clock accuracy through incorporating the crosslink data with station data was quantified. Analysis revealed that the inclusion of crosslink data with station data is equivalent to the inclusion of additional stations. In particular, the low noise levels associated with the derived clock observations will improve the quality of the precise clock estimates.

14. SUBJECT TERMS			15. NUMBER OF PAGES
National Imagery and Mapping Agency (NIMA) Crosslink Ranging Data	Orbit and Clock Accuracy		45
			16. PRICE CODE
17. SECURITY CLASSIFICATION OF REPORTS	18. SECURITY CLASSIFICATION OF THIS PAGE	19. SECURITY CLASSIFICATION OF ABSTRACT	20. LIMITATION OF ABSTRACT
UNCLASSIFIED	UNCLASSIFIED	UNCLASSIFIED	UL

FOREWORD

The GPS Block IIR and IIF satellites will generate satellite-to-satellite range measurements for on-board navigation with the Autonomous Navigation System (AutoNav). With the availability of crosslink data through the GPS Master Control Station (MCS), these data could be included with station tracking data in the generation of precise orbit and clock estimates. This report documents the expected improvements in the National Imagery and Mapping Agency (NIMA) orbit and clock estimates with the inclusion of crosslink ranging data. This work was funded by the NIMA and was performed in the Space Systems Applications Branch, Space and Weapons Systems Analysis Division, Theater Warfare Systems Department.

This report has been reviewed by Dr. Jeffrey N. Blanton, Head, Space Systems Applications Branch; and James L. Sloop, Head, Space and Weapons Systems Analysis Division.

Approved by:

RICHARD T. LEE, Acting Head
Theater Warfare Systems Department

CONTENTS

ILLUSTRATIONS

CONTENTS (Continued)

TABLES

TABLES (Continued)

INTRODUCTION

As Block IIR and IIF satellites are launched to replenish the GPS constellation, it is anticipated that at some point in the future, crosslink data between these satellites will be collected and eventually used for on-board navigation. It is expected that the Autonomous Navigation System will be able to broadcast satellite position and clock data with a User Range Error (URE) of less than 1.8 m with minimal ground contact. Within this framework, each satellite will transmit UHF ranging signals at two frequencies. All visible satellites will make pseudorange measurements to this transmitting satellite. In addition, each satellite will also send and receive pseudorange measurement values and additional information from all other visible satellites. This will allow measurement preprocessing resulting in two derived measurements in which the ephemeris and clock are decoupled, producing a distance measurement and a clock bias measurement. These measurements will then be processed onboard each satellite using Kalman filters to arrive at new position and clock estimates for the purpose of generating improved navigation messages.

With the availability of the crosslink data stream for processing at the GPS Master Control Station through 24-hour dumps and appropriate data reformatting and preprocessing software in place, it will be possible to incorporate these data types along with station tracking data into the generation of precise orbit and clock estimates. Extensive modifications, based on the formulation given in Reference 1, have been made to allow the Multisatellite Filter/Smoother system of programs within OMNIS to process crosslink ranging data. The goal of this crosslink ranging study was to gain an understanding, through data simulations, of the characteristics and relative information content of the crosslink data types. With this knowledge, the overall achievable orbit and clock accuracy through incorporating the crosslink data with station tracking data has been quantified.

SIMULATIONS

STATION TRACKING SIMULATIONS

The simulated station data case created for a previous study was enhanced to reflect the orbit and clock accuracy associated with NIMA production as of late 1997. Station tracking data of GPS were simulated for an 18-station network covering 5 days to allow for three overlapping 3-day fit spans, with the middle day of each fit span used for analysis. The 12-station network consisted of the five Air Force tracking sites and seven NIMA tracking sites. Additional tracking sites to complete the 18-station network included Thule, Greenland; Anchorage, Alaska; Omsk, Russia; Pretoria, South Africa; Tahiti; and McMurdo, Antarctica. These last six sites were based on discussions with NIMA a few years ago about possible future sites for additional tracking stations. NIMA has recently deployed sites at Eielson AFB, Alaska; Wellington, New Zealand; and Pretoria, South Africa. Figure 1 gives the names and locations of the 12-station baseline network sites. Figures 2 gives the 18-station future network sites.

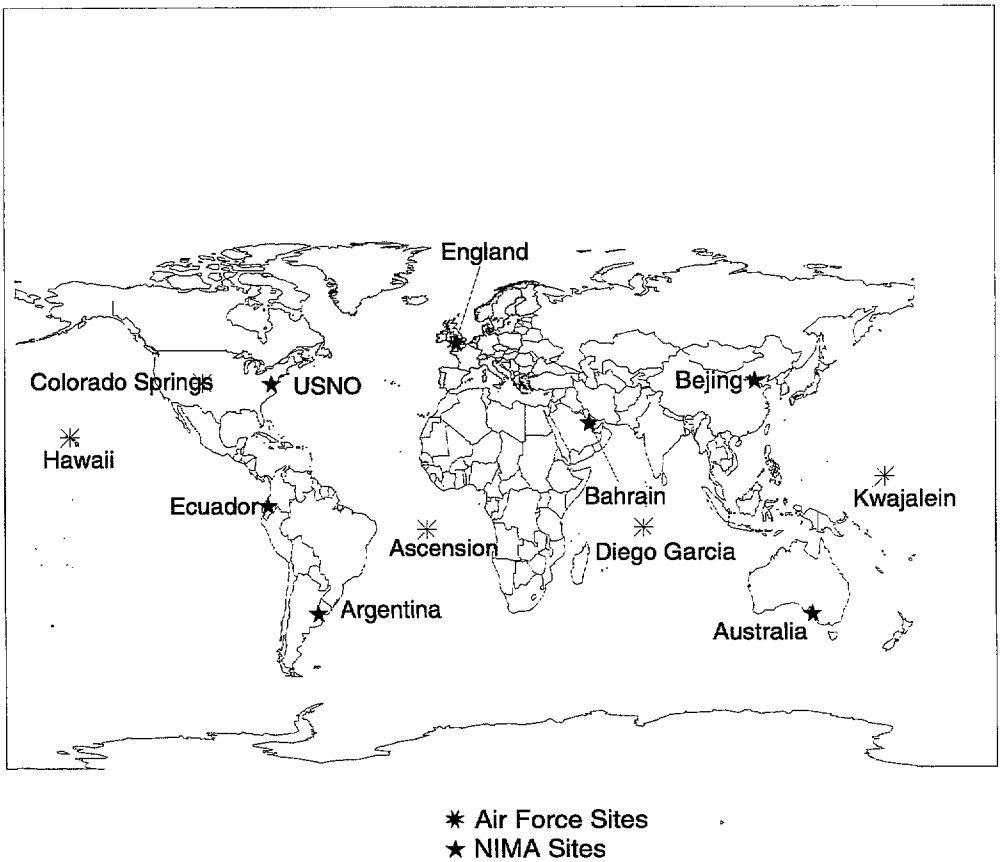

FIGURE 1. 12-STATION BASELINE NETWORK FOR SIMULATIONS

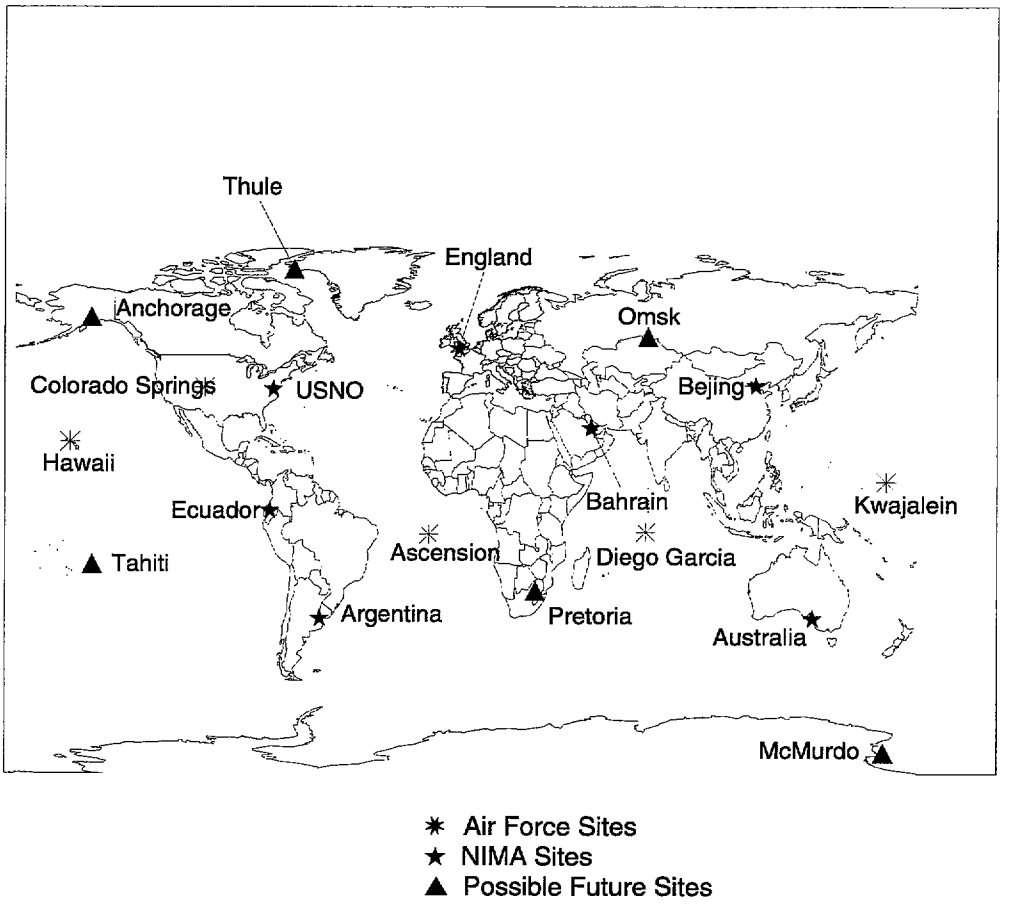

FIGURE 2. 18-STATION FUGURE NETWORK FOR SIMULATIONS

The nominal 24-satellite GPS constellation was simulated. For 22 of the satellites, the initial conditions for integrating the "truth" trajectories were obtained from the actual trajectories for day 320 of 1993. This included the radiation pressure scale factor and y-axis acceleration values. For the other two satellites, the initial conditions were based on adjusting the orbital elements for satellites nearby in the same orbit planes. PRN4 was defined to be in the D4 slot and used PRN24's elements (D1 slot) with 32.13 deg added to its mean anomaly. PRN6 was defined to be in the C1 slot and used PRN28's elements (C2 slot) with 100.08 deg added to its mean anomaly. These mean anomaly separations came from a nominal set of elements generated by the Aerospace Corporation to support GPS constellation management studies.

The actual radiation pressure scale factor and y-axis acceleration values for PRNs 24 and 28 were used for PRNs 4 and 6, respectively. "Truth" trajectories for all 24 satellites were integrated using an integration interval of 300 sec, except for the eclipse transition regions when the interval was decreased to 10 sec. The trajectories were written at a 900-sec time interval. Reference trajectories for all 24 satellites were integrated using different force models and Earth orientation

than those used for the "truth" trajectories to simulate error sources. To avoid any linearity problems, the reference trajectories where then fit to the "truth" trajectories using least squares and reintegrated to provide the final reference trajectories. Table 1 gives the force models and Earth orientation information selected for the "truth" and reference trajectories. The IERS solid earth tidal potential model without the frequency dependent term was used and no ocean tide model was used. The T20 radiation pressure model includes effects of the plume shield and thermal re-radiation pressure not included in the ROCK42 model. No Earth albedo model was used. The angle between the satellite-sun vector and the y-axis acceleration set not equal to 90 deg causes a small component of the y-axis acceleration to be added to the body-fixed x component of the radiation pressure acceleration and the y-axis value is decreased slightly. Tables 2 and 3 give the daily x, y, and UT1-UTC values from the IERS and values based on the appropriate NIMA coefficient sets, respectively. For the 3 days of interest the largest differences in x and y correspond to about 12 and 7 cm at the Earth's surface, respectively. For UT1-UTC the rate of change is the only quantity that can be compared with the IERS final values. The worst case difference in the change in UT1-UTC over a day was 0.35 msec, which corresponds to approximately 18 cm at the Earth's surface. Quadratic interpolation in these tables was used to determine the Earth orientation values at any given time.

TABLE 1. FORCE MODELS AND EARTH ORIENTATION USED FOR THE GPS "TRUTH" AND REFERENCE TRAJECTORIES

Force Models	Truth	Reference
Gravity Field	JGM-2, 20x20 A_{Earth} = 6378.136 km $C_{2,1} = -.17 \times 10^{-9}$, $S_{2,1} = 1.19 \times 10^{-9}$	WGS 84, 8x8 A_{Earth} = 6378.137 km $C_{2,1} = 0$, $S_{2,1} = 0$.
GM	398600.4415 km^3/s^2	398600.4423 km^3/s^2
Sun/Moon	Point mass models DE200/LE200 ephemerides	Point mass models DE200/LE200 ephemerides
Tides	Solid earth, k_2 = 0.30	Solid earth, k_2 = 0.29
Radiation pressure	T20 model (Reference 2), Nominal scale factor + Varying cross-sectional area modeled as Gauss-Markov process with steady-state sigma = 5% and tau = 15 min Earth radius for eclipse model = 6278.137 km	ROCK42 model Adjusted scale factor Constant cross-sectional area Earth radius for eclipse model = 6378.137 km
Y-axis acceleration	Nominal value + Additional acceleration modeled as Gauss-Markov process with steady-state sigma = 5% and tau = 15 min Angles between sat-sun vector and y-axis randomly perturbed between 88 and 92 degrees	Adjusted value Angle between sat-sun vector and y-axis = 90 degrees
Earth Orientation	IERS final values (see Table 2)	NIMA coefficients + zonal tide effects on UT1-UTC with periods up to 35 days (see Table 3)

TABLE 2. IERS FINAL EARTH ORIENTATION VALUES FOR 6 DAYS USED FOR "TRUTH" TRAJECTORIES

Day #	x (")	y (")	UT1-UTC (s)
320	-0.0485	0.4385	0.30652
321	-0.0477	0.4394	0.30429
322	-0.0470	0.4404	0.30204
323	-0.0464	0.4415	0.29974
324	-0.0459	0.4426	0.29737
325	-0.0453	0.4437	0.29496

TABLE 3. NIMA EARTH ORIENTATION VALUES FOR 6 DAYS USED FOR REFERENCE TRAJECTORIES

Day #	x (")	y (")	UT1-UTC (s)
320	-0.0482	0.4369	0.30416
321	-0.0467	0.4378	0.30164
322	-0.0452	0.4487	0.29907
323	-0.0436	0.4395	0.29642
324	-0.0420	0.4404	0.29370
325	-0.0404	0.4412	0.29091

Simulated pseudorange and range difference observations for the 18 stations were generated for a 5-day time span using the "truth" GPS trajectories and other criteria as specified in Table 4. It was assumed that residual ionospheric refraction and multipath effects were part of the measurement noise. The observation sigmas used in NIMA production were conservative compared to the level of measurement noise introduced through the simulator. For 16 of the 24 satellites the simulated clock noise was based on Allan variances computed using the NIMA precise clock estimates for 22 weeks from 1993 (see Reference 3). Of the remaining 8 satellites, the noise for 5 was based on the Allan variances computed for PRN25. This satellite was the only Block II operating on a rubidium frequency standard for the clock estimates analyzed. PRN25 is in the A plane. The other 5 satellites that have clock noise based on this Allan variance were selected so that there was only one satellite in each orbit plane. These satellites are PRNs 4, 5, 6, 23, and 29. Clock noise based on an average Allan variance for cesium clocks (corresponding to a stability of 1.2×10^{-13} at 10^5 sec) was used for the other 3 satellites, PRNs 7, 9, and 31. The station clock noise was based on Allan variance specifications for the HP5061A cesium clock (corresponds to stability of 2.8×10^{-14} at 10^5 sec). Table 5 gives the two white noise spectral densities required by the clock model for all

GPS satellites and stations. Table 6 gives the two white noise spectral densities used in OMNIS when estimating clocks in the second filter stage. It should be noted that differences exist between the white noise spectral densities used in OMNIS for these simulations and those used in NIMA production. The satellite spectral densities selected for use in OMNIS for these simulations are also categorized as either rubidium, cesium, or other standard, with the actual values for the rubidium standard slightly different from NIMA production. Also, the assignment of specific satellites to each category is different. These differences were required to ensure that the spectral clock densities used for estimating clocks in OMNIS remained conservative with respect to the clock noise added to the simulated observations. The spectral densities for the 6 future site clocks were grouped with Colorado Springs (CS) and the 7 NIMA site clocks. No time tag errors, antenna offset errors, or data dropouts were simulated.

TABLE 4. SIMULATED GPS STATION OBSERVATION INFORMATION

Number of stations	18 (see Figure 2)
Types of obs.	Pseudorange, range difference
Data rates	900 sec
Viewing restrictions	All-in-view receivers with min. elev. angle = 10 degrees
Measurement noise	White, Gaussian noise with sigmas of 30 cm on pseudorange, 1 cm (correlated) on range difference
GPS satellite clocks	Stochastic phase noise based on computed Allan variances (see Table 5) + quadratic polynomial, nominal offsets from OMNIS Editor
Station clocks	Stochastic phase noise based on specification Allan variance (see Table 5) + linear polynomial, nominal offsets from OMNIS Editor; The NIMA
site	at USNO designated as the master station for clock estimation
Tropospheric refraction error	Hopfield with default weather - Chao with perturbed weather Temperature perturbation amplitudes from 7 to 12 degrees C Pressure perturbation amplitudes from 5 to 13 millibars Relative humidity perturbation amplitudes from 4 to 24 percent Amplitudes of azimuth sinusoids for pressure and relative humidity perturbations same as above
Station coordinates	Randomly perturbed in ENV frame with one sigma = 5 cm East perturbations varied from -7 to +16 cm North perturbations varied from -9 to +8 cm Vertical perturbations varied from -9 to +10 cm Unperturbed coordinates used in OMNIS

TABLE 5. CLOCK MODEL WHITE NOISE SPECTRAL DENSITIES FOR GPS SIMULATIONS

PRN#	White noise spectral density on freq. offset state ($x10^{-20}$ ppm^2/sec)	White noise spectral density on time offset state ($x10^{-09}$ $\mu sec^2/sec$)
1	5.1641	1.9695
2	1.1082	1.6248
4	2.1168	0.5645
5	2.1168	0.5645
6	2.1168	0.5645
7	2.0000	1.4400
9	2.0000	1.4400
14	1.4281	1.0139
15	2.8466	1.1495
16	1.8467	3.8715
17	1.2092	1.2564
18	1.3534	1.5048
19	1.9192	1.3240
20	3.4620	2.3063
21	13.6840	3.4064
22	1.6021	1.2884
23	2.1168	0.5645
24	1.2420	1.1255
25	2.1168	0.5645
26	5.1641	1.9695
27	1.5992	1.3036
28	0.7350	0.8208
29	2.1168	0.5645
31	2.0000	1.4400
All stations	1.2000	0.0400

TABLE 6. CLOCK MODEL WHITE NOISE SPECTRAL DENSITIES FOR OMNIS PROCESSING

Clock Groups	White noise spectral density on freq. offset state ($x10^{-20}$ ppm^2/sec)	White noise spectral density on time offset state ($x10^{-09}$ $\mu sec^2/sec$)
Cesium	100.0000	3.0000
Rubidium	11.1000	0.6000
Other	1110.0000	20.0000
CS, 7 NIMA, and 6 Future sites	4.4450	0.3000
4 Other Air Force sites	4.4450	1.1100

Using 5 days of data for both 12- and 18-station networks, precise orbit and clock estimates were generated for 3 three-day fit spans. Each set of fits was based on processing the simulated pseudorange and range difference data using NIMA production methods (2-stage filter) with "tuned" *a priori* and process noise statistics and the improved tropospheric refraction model (see Reference 4). The overall statistics compiled from the middle day of the three 3-day fits from the 12-station network established a baseline case, and from the 18-station network established a future benchmark for comparisons. Tables 7 and 9 give the clock and orbit differences from the "truth" for each set of estimates for the middle day of each fit and overall, for the 12-station and 18-station cases, respectively. The RMS was taken over all 24 satellites and the peak was the maximum deviation from the mean for any satellite at any time, with the sign indicating direction. Tables 8 and 10 give the total, orbit, and clock UREs for the middle day of each fit and overall, for the 12-station and 18-station cases, respectively, with these results summarized in Figure 3. These are computed using the equation

$$\text{RMS URE} = [(\text{Radial} - \text{Clock})^2 + 1/49(\text{Along-track}^2 + \text{Cross-track}^2)]^{1/2}$$

This equation represents an analytical expression used to compute combined orbit and clock errors for a particular satellite, in an RMS sense, as seen by an average ground user. The RMS was taken over a 24-hour span for each satellite and combined to get an overall statistic. The peak was the worst case for the RMS of any satellites at any particular time. The correlation reported represents the correlation between the radial orbit differences and the clock differences. The orbit RMS URE for ground users was 10.5 cm for the 12-station network and 7.8 cm for the 18-station network. The RMS after-fit residuals combined over the 3 days for the 12-station case were 23.8 cm for the pseudorange data and 0.9 cm for the range difference data. For the 18-station case the RMS after-fit residuals combined over the 3 days were 25.4 cm for the pseudorange data and 1.1 cm for the range difference data.

TABLE 7. GPS CLOCK AND ORBIT DIFFERENCES VS. "TRUTH" FOR 12-STATION BASELINE CASE (CM)

Day #	Clock			Radial			Along-Track			Cross-Track		
	Mean	RMS	Peak	Mean	RMS	Peak	Mean	RMS	Peak	Mean	RMS	Peak
321	6.8	23.2	-105.4	3.2	8.8	25.8	-3.4	27.2	-60.7	-1.8	17.9	-45.1
322	7.8	23.5	95.8	2.9	10.1	-30.1	-5.0	28.0	-72.6	-0.4	17.4	-40.3
323	5.6	23.2	-95.4	2.6	9.1	30.5	-5.9	26.5	-64.9	-0.9	18.0	-42.6
All	6.7	23.2	-105.4	2.9	9.3	30.5	-4.8	27.2	-72.6	-1.0	17.8	-45.1

TABLE 8. URES FOR 12-STATION BASELINE CASE (CM)

Day #	Total		Orbit		Clock		Corr(R,C)
	RMS	Peak	RMS	Peak	RMS	Peak	
321	21.2	93.5	10.0	28.7	23.2	104.0	0.400
322	20.9	104.4	11.2	30.6	23.5	106.5	0.452
323	21.1	86.5	10.2	32.7	23.2	99.9	0.429
All	21.1	104.4	10.5	32.7	23.3	106.5	0.427

TABLE 9. GPS CLOCK AND ORBIT DIFFERENCES VS. "TRUTH" FOR 18-STATION FUTURE CASE (CM)

Day #	Clock			Radial			Along-Track			Cross-Track		
	Mean	RMS	Peak	Mean	RMS	Peak	Mean	RMS	Peak	Mean	RMS	Peak
321	5.4	21.1	-89.7	3.0	6.5	18.9	-2.4	19.8	58.3	-1.7	18.2	51.6
322	5.4	20.4	-102.9	2.8	7.1	21.2	-3.1	19.6	-40.2	-0.5	17.4	-52.4
323	3.6	20.1	-88.0	2.8	6.9	22.3	-4.1	20.0	-43.2	-0.9	18.1	-54.4
All	4.8	20.5	-102.9	2.9	6.8	22.3	-3.2	19.8	58.3	-1.0	17.9	-54.4

TABLE 10. URES FOR 18-STATION FUTURE CASE (CM)

Day #	Total		Orbit		Clock		Corr(R,C)
	RMS	Peak	RMS	Peak	RMS	Peak	
321	19.8	87.8	7.6	25.1	21.1	89.4	0.333
322	18.6	103.0	8.0	23.2	20.4	102.1	0.402
323	18.8	88.8	7.9	24.0	20.1	88.7	0.369
All	19.1	103.0	7.8	25.1	20.5	102.1	0.368

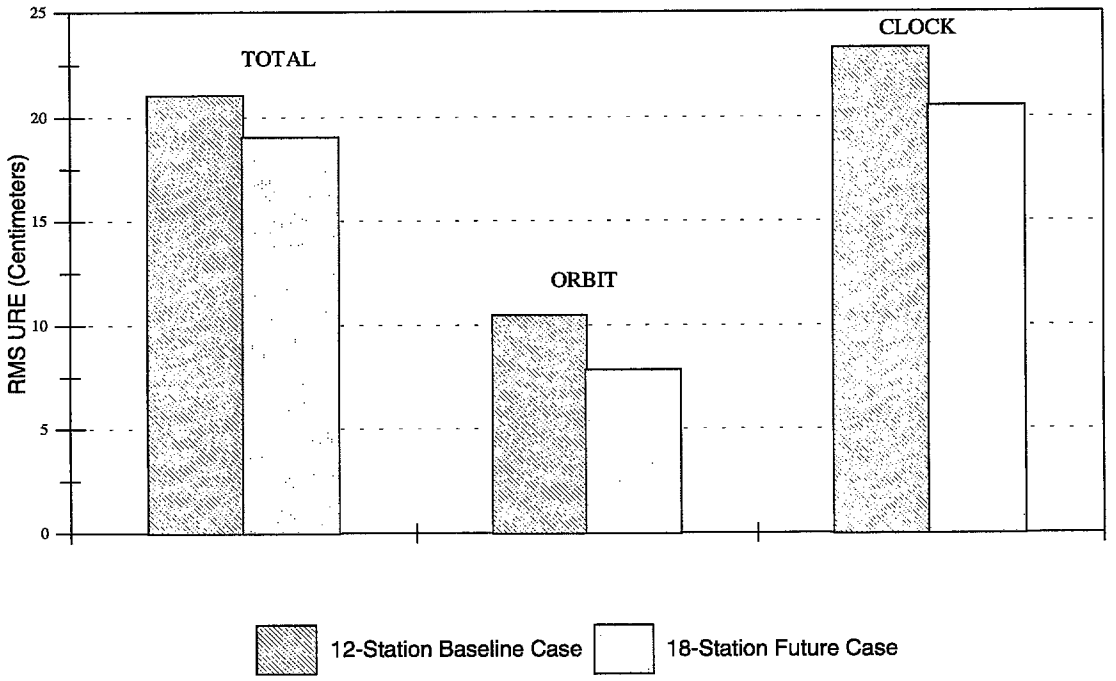

FIGURE 3. RMS URES FOR STATION TRACKING DATA

The level of the errors incorporated into the simulated data were selected to emulate precise orbit and clock accuracy associated with NIMA production. When this study was begun, the predicted error levels for the NIMA orbit estimates was expected to be around 10 cm. A level of 8 cm was achieved operationally. The reported orbit and clock differences from "truth" along with the total, orbit, and clock UREs support a claim that the simulated data for the 12-station baseline case are realistic. Given that the reported statistics from the simulated 18-station case can not be compared against a similar set of NIMA precise orbits and clocks derived from a 18-station network and the study conducted by NSWCDD on GPS orbit accuracy gain to be expected by deploying additional NIMA stations (see Reference 5) is not entirely consistent with NIMA production techniques, it is not known if the simulated 18-station case is realistic. However, given the accuracy of NIMA precise orbits and clocks, it is felt that the improvement seen in the simulated 18-station case as compared to the simulated 12-station case is reasonable.

CROSSLINK RANGING SIMULATIONS

Simulated crosslink ranging data for the 24 GPS satellites including pseudorange data (type 3), derived distance data (type 4), and derived clock data (type 5), were generated for the 5-day span using the "truth" GPS trajectories, nominal satellite clock offsets, satellite clock noise based on Table 5, and other criteria as specified in Table 11. Dual-frequency corrected pseudoranges are formed through combining dual UHF frequency signals. For the purpose of these simulations, the higher UHF frequency was selected to be 300 MHZ and the lower UHF frequency was selected to be 283.5 MHZ. The single-frequency pseudorange measurement noise was selected to be 33 cm (Reference 6). As the UHF frequency signals are combined in the formation of the dual-frequency pseudoranges, the single-frequency measurement noise must be multiplied by a relatively large scale factor based upon this combination to get the proper measurement noise. Dual-frequency corrected pseudoranges between a satellite pair are used to derive a measurement in which the ephemeris is decoupled from the clock. This derived distance measurement is formed through averaging the pseudoranges between a satellite pair, removing common clock biases. The measurement noise is based upon the dual-frequency pseudorange measurement noise value. The derived clock measurements are formed through differencing pseudoranges between a satellite pair and dividing by 2, resulting in a clock bias difference measurement. For this derived measurement, single frequency pseudorange measurements are used. The measurement noise levels are reported in Table 12. The measurements between a satellite pair are assumed to be simultaneous. In the actual crosslink implementation, each satellite is assigned a 1.5-sec transmitting slot in a 36-sec interval at the beginning of each 15-min segment.

TABLE 11. SIMULATED GPS CROSSLINK OBSERVATION INFORMATION

Number of satellites	24
Types of obs.	Pseudorange, derived distance, derived clock
Data rates	900 sec
Viewing restrictions	Antenna visibility for a satellite pair constrained to be between -32 and -65 deg as measured from each satellite's local horizon
Measurement noise	White, Gaussian noise with a single-frequency pseudorange sigma of 33 cm
GPS satellite clocks	Stochastic phase noise based on computed Allan variances (see Table 5) + quadratic polynomial, nominal offsets from OMNIS Editor
Crosslink Biases	Bias with a 12 hr periodic; unique random bias, amplitude, and phasing for the transmitter and receiver for each satellite

TABLE 12. MEASUREMENT NOISE LEVELS FOR GPS CROSSLINK OBSERVATIONS

Data Type	Measurement Noise (cm)
Crosslink Pseudorange	413.6
Crosslink Derived Distance	292.4
Crosslink Derived Clock	23.3

Transmitter and receiver delays between the point in the satellite where the clock is common to the L-band transmitter and UHF transmitter and receiver circuitry and their respective antenna phase centers exists for each satellite and are referred to as crosslink biases (see Reference 7). The crosslink biases were implemented within the simulator as a bias plus a 12-hr periodic. For each satellite, a bias, amplitude, and phasing unique for the transmitter and receiver were defined. The mean of the receiver biases over all of the satellites was 4.0 ns, the mean of the transmitter biases was 2.5 ns, the mean of the receiver amplitudes was 1.3 ns, and the mean of the transmitter amplitudes was 1.0 ns. The phasings of the transmitter and receiver periodics were also unique and were treated as either random or common. No time tag errors, antenna offset errors, or data dropouts were simulated. No tropospheric refraction errors were introduced as the viewing restrictions prevent the crosslink data from ever passing through the troposphere. Also, as the crosslink data has no direct link to the ground, there is no information content related to Earth orientation.

Estimated Parameters vs. Data Types

To better understand what satellite-related clock and crosslink bias parameters can be estimated with crosslink data types by themselves or in combination with station tracking data, a simulated case was generated in which only satellite and station time offset biases and crosslink biases were present. In addition the correct level of measurement noise was added to each data type. This was a three-day case that included station pseudorange (type 0), crosslink pseudorange (type 3), crosslink derived distance (type 4), and crosslink derived clock (type 5) data at 15-min intervals. The master station had zero time offset error as did one of the satellites. The crosslink receiver bias was set to zero for this same satellite also. Setting errors to zero was done to make comparisons of the estimated biases with the actual biases easier. In all Filter runs, only time offsets were estimated and only as biases. The same was true for the crosslink bias parameters. The first crosslink bias parameter is the receiver bias and the second is the difference between the transmitter and receiver biases. Table 13 summarizes what parameters can be estimated for the various combinations of data types and depending on whether satellite clock estimates are available or are not available. Since types 4 and 5 measurements are derived from pairs of type 3 measurements, type 3 measurements are never processed with the other two. Data type 4 contains no information on satellite clock parameters and no information on the crosslink receiver biases. If station data (type 0) are being processed, satellite clock parameters would always be estimated with one station's clock treated as the master clock.

TABLE 13. ESTIMATED PARAMETERS VS. DATA TYPES

Data Types	Sat Clock Estimates Available	Satellite Clock	Crosslink Receiver Bias	Crosslink Trans.-Rec. Bias
3	N	Y*	N	Y
	Y	N	Y*	Y
0,3	N	Y	Y*	Y
4	-	-	N	Y
0,4	N	Y	N	Y
5	N	Y*	N	N
	Y	N	Y*	N
	Y	N	N	Y*
0,5	N	Y	N	Y*
	N	Y	Y*	N
4,5	N	Y*	N	Y
	Y	N	Y*	Y
0,4,5	N	Y	Y*	Y

N = No Y = Yes Y* = Yes with parameter(s) deweighted for one Satellite

Treatment of Crosslink Biases

Simulated station and crosslink ranging data were merged for the purpose of deriving orbit and clock estimates under different assumptions. For the first day, 3-day fits were performed with the middle day of the fit used to determine relative GPS orbit and clock accuracy and quantify the effects of the various experiments. The estimation technique used was identical to the NIMA production method (2-stage filter) with "tuned" a priori and steady-state sigmas and the improved tropospheric refraction model (see Reference 4). All fits were conducted with the 12-station baseline network station-tracking data. Data combinations investigated include merged station-tracking pseudorange and range difference observations with crosslink pseudorange observations (types 0, 9, and 3), merged station-tracking pseudorange and range difference observations with crosslink derived distance and clock observations (types 0, 9, 4, and 5), merged station-tracking pseudorange and range difference observations with crosslink derived distance observations (types 0, 9, and 4), and merged station-tracking pseudorange and range difference observations with crosslink derived clock observations (types 0, 9, and 5). The observation sigmas used are given in Table 14. Although the observation sigmas for the station-tracking data were conservative with respect to the level of measurement noise introduced through the simulator, the measurement noise and observation sigmas assigned to the crosslink ranging observations were identical. The phasing of the transmitter and receiver delays incorporated into the crosslink ranging data through the simulator was random for these experiments.

TABLE 14. OBSERVATION SIGMAS

Data Type	Sigma (cm)
Station-tracking Pseudorange Colorado Springs 7 NIMA, 4 other Air Force, 6 Future Sites	 100.0 40.0
Station-tracking Range Difference	1.5
Crosslink Pseudorange	413.6
Crosslink Derived Distance	292.4
Crosslink Derived Clock	23.3

Additional parameters for each satellite, the crosslink biases, were estimated with the inclusion of the crosslink observations. The first crosslink bias parameter is the receiver bias and the second crosslink bias parameter is the difference between the transmitter and receiver biases. Estimation of satellite-related clock and crosslink bias parameters with respect to the various data combinations was consistent with Table 13. To first understand the behavior and relationship of the crosslink biases with the satellite clocks, experiments with various treatments of the crosslink bias parameters within the filter were conducted. The sensitivity of the statistical assumptions appropriate for each treatment of the crosslink biases was also investigated. Treatments of the crosslink biases include unconstrained in the first-stage filter and as Gauss-Markov processes in the second-stage filter, Gauss-Markov processes in the first- and second-stage filters, and as a random walk in each stage. Treatment of the crosslink biases as unconstrained in the first-stage filter refers to implementation of large *a priori* and steady-state sigmas identical to those used with the clock parameters. During the course of this analysis, it became apparent that not all of the sensitivity experiments conducted could be reported. For the purpose of demonstrating the sensitivity of the orbit and clock estimates to the various treatments and statistical assumptions, a subset of all experiments performed was selected. Table 15 summarizes these sensitivity experiments. Also, it became apparent that not all of the sensitivity experiments were pertinent for each of the data type combinations, and therefore many are not reported.

TABLE 15. TREATMENT OF CROSSLINK BIASES AND STATISTICAL ASSUMPTIONS

Treatment of Crosslink Biases	Statistical Assumptions		Case
	First-stage filter	Second-stage filter	
Crosslink biases unconstrained in first-stage, Gauss-Markov processes in the second-stage filter	AP = 0.1111×10^{-02} ns VR = 0.1111×10^{-02} ns^2/sec	AP = 5 ns, SS = 5 ns, T = 4 hrs	A
		AP = 5 ns, SS = 0.75 ns, T = 4 hrs	B
		AP = 5 ns, SS = 0.25 ns, T = 4 hrs	C
Gauss-Markov processes in the first- and second-stage filters	AP = 5 ns, SS = 5 ns, T = 4 hrs	AP = 5 ns, SS=5 ns, T = 4 hrs	D
	AP = 5 ns, SS = 0.75 ns, T = 4 hrs	AP = 5 ns, SS = 0.75 ns, T = 4 hrs	E
	AP = 5 ns, SS = 0.25 ns, T = 4 hrs	AP = 5 ns, SS = 0.25 ns, T = 4 hrs	F

(AP = *A Priori*, VR = Variance Rate, SS = Steady-State Sigma, T = Tau)

Tables 16 through 23 represent the sensitivity of the orbit and clock estimates to different treatments of the crosslink biases and various assumed statistics for each of the data combinations. Orbit and clock differences from "truth" for the middle day of each fit are presented in Tables 14, 16, 18, and 20 for types 0, 9, and 3; types 0, 9, 4, and 5; types 0, 9, and 4; and types 0, 9, and 5, respectively. The total, orbit, and clock UREs for the middle day of each fit are presented in Tables 15, 17, 19, and 21 for the same collections of data types, respectively. For comparison purposes, the overall orbit and clock differences from "truth" for the ground-tracking observations for the middle day of each of the 3 fits and the total, orbit, and clock UREs for the ground-tracking observations for the middle day of each of the 3 fits are included in the appropriate tables. The differences for these cases are referred to as Case 12.

These tables indicate that fits based on using data types 0, 9, 4, and 5 together (Case E) resulted in precise orbit and clock estimates which most closely agree with "truth". Small reductions in both orbit and clock UREs with respect to the 12-station baseline case were noted, with a decrease in the RMS total URE from 21.2 cm to 18.4 cm. These reductions were attributed to a decrease in along-track orbit errors and an improvement in clock estimation. The along-track RMS differences decreased from 27.2 cm to 21.8 cm and the clock RMS differences decreased from 23.2 cm to 20.2 cm. The addition of the derived distance measurements and, in particular, the derived clock measurements, with its corresponding reduced noise level, together provided additional information responsible for these reductions.

Fits based on using the other data types resulted in improved orbit and clock estimates as well, but they did not agree as well with "truth" as orbit and clock estimates based on using data types 0, 9, 4, and 5. Fits based on using data types 0, 9, and 3 resulted in precise orbit estimates which agreed with "truth" at the same level as estimates based on using data types 0, 9, 4, and 5, but the clock estimates did not agree as well with "truth". Fits based on using data types 0, 9, and 5 resulted in improved clock estimates, but again, they did not agree with "truth" as well as clock estimates based on using data types 0, 9, 4, and 5. Fits based on using data types 0, 9, and 4 resulted in improved orbits, but they did not agree with "truth" as well as orbit estimates based on using data types 0, 9, 4, and 5 or data types 0, 9, and 3.

The greatest sensitivity with respect to the *a priori* and steady-state sigmas associated with the crosslink biases was seen in the experiments with data types 0, 9, and 5 followed by the experiments with data types 0, 9, 4, and 5. This sensitivity is due to the reduced noise level associated with the derived clock data. Very little sensitivity was seen in the experiments with data types 0, 9, and 4. Small differences were seen when the crosslink biases were treated as a Gauss-Markov process versus unconstrained in the first-stage. Again, the experiments with data types 0, 9, and 5 and data types 0, 9, 4, and 5 exhibited the largest differences with respect to the treatment of the crosslink biases as Gauss-Markov process versus unconstrained in the first-stage. The largest differences were noted with the experiments using smaller steady-state sigmas. The *a priori* and steady-state sigmas resulting in the best agreement with "truth" using data types 0, 9, and 3 or data types 0, 9, and 5 were higher (5 ns for both *a priori* and steady-state sigmas) versus the statistics resulting in the best agreement with "truth" using data types 0, 9, 4, and 5 (5 ns *a priori* and 0.75 ns steady-state sigmas).

Experiments with the treatment of the crosslink biases as random walk processes were conducted with each data combination. As there was generally similar agreement with "truth" as with the Gauss-Markov treatment, these results are not reported.

TABLE 16. GPS CLOCK AND ORBIT DIFFERENCES VS. "TRUTH" FOR DATA TYPES 0, 9, AND 3 (CM)

Case	Clock			Radial			Along-Track			Cross-Track		
	Mean	RMS	Peak	Mean	RMS	Peak	Mean	RMS	Peak	Mean	RMS	Peak
12	6.8	23.2	-105.4	3.2	8.8	25.8	-3.4	27.2	-60.7	-1.8	17.9	-45.1
A	6.9	22.8	-98.2	3.1	8.1	24.8	-4.8	21.8	-46.2	-1.8	17.6	-46.4
B	7.4	22.9	-95.0	3.1	8.1	24.8	-4.8	21.8	-46.2	-1.8	17.6	-46.4
C	7.7	22.9	-94.0	3.1	8.1	24.8	-4.8	21.8	-46.2	-1.8	17.6	-46.4
D	6.8	22.8	-99.3	3.0	8.1	22.5	-5.0	21.6	-46.3	-1.8	17.6	-47.4
E	7.3	22.9	-98.1	3.0	8.0	20.6	-5.0	21.3	55.1	-1.8	18.1	-47.8
F	7.6	22.9	-96.7	3.1	8.0	21.2	-5.1	21.5	55.5	-1.8	18.3	-47.4

TABLE 17. URES FOR DATA TYPES 0, 9, AND 3 (CM)

Case	Total		Orbit		Clock		Corr(R,C)
	RMS	Peak	RMS	Peak	RMS	Peak	
12	21.2	93.5	10.0	28.7	23.2	104.0	0.400
A	21.0	90.9	9.1	27.7	22.8	97.1	0.366
B	21.2	86.5	9.1	27.7	22.9	96.5	0.339
C	21.3	84.6	9.1	27.7	22.9	97.7	0.328
D	21.0	91.1	9.0	25.3	22.8	98.6	0.364
E	21.2	87.2	8.9	24.0	22.9	98.1	0.334
F	21.3	84.8	8.9	24.7	22.9	100.2	0.326

TABLE 18. GPS CLOCK AND ORBIT DIFFERENCES VS. "TRUTH" FOR DATA TYPES 0, 9, 4, AND 5 (CM)

Case	Clock			Radial			Along-track			Cross-track		
	Mean	RMS	Peak	Mean	RMS	Peak	Mean	RMS	Peak	Mean	RMS	Peak
12	6.8	23.2	-105.4	3.2	8.8	25.8	-3.4	27.2	-60.7	-1.8	17.9	-45.1
A	6.9	22.2	-96.8	3.1	8.1	24.7	-4.8	21.8	-46.2	-1.8	17.6	-46.4
B	8.1	20.2	-85.9	3.1	8.1	24.7	-4.8	21.8	-46.2	-1.8	17.6	-46.4
C	10.7	23.2	-93.8	3.1	8.1	24.7	-4.8	21.8	-46.2	-1.8	17.6	-46.4
D	6.8	22.2	-98.1	3.0	8.1	22.5	-5.2	21.7	-47.0	-1.8	17.7	-47.4
E	7.8	20.2	-86.3	3.0	7.9	23.1	-5.7	21.7	57.1	-1.8	18.6	-48.6
F	9.6	24.0	-96.7	3.0	9.8	30.2	-5.8	24.7	67.1	-1.8	19.4	-48.7

TABLE 19. URES FOR DATA TYPES 0, 9, 4, AND 5 (CM)

Case	Total		Orbit		Clock		Corr(R,C)
	RMS	Peak	RMS	Peak	RMS	Peak	
12	21.2	93.5	10.0	28.7	23.2	104.0	0.400
A	20.3	89.4	9.1	27.6	22.2	95.6	0.378
B	18.5	82.8	9.1	27.6	20.2	84.5	0.349
C	22.4	91.4	9.1	27.6	23.2	91.4	0.162
D	20.3	89.9	9.0	25.4	22.2	97.3	0.377
E	18.4	81.7	8.9	26.1	20.2	85.0	0.373
F	20.6	88.3	10.8	33.2	24.0	92.7	0.514

TABLE 20. GPS CLOCK AND ORBIT DIFFERENCES VS. "TRUTH" FOR DATA TYPES 0, 9, AND 4 (CM)

Case	Clock			Radial			Along-track			Cross-track		
	Mean	RMS	Peak	Mean	RMS	Peak	Mean	RMS	Peak	Mean	RMS	Peak
12	6.8	23.2	-105.4	3.2	8.8	25.8	-3.4	27.2	-60.7	-1.8	17.9	-45.1
A	6.8	22.9	-99.1	3.1	8.1	24.7	-4.8	21.8	-46.2	-1.8	17.6	-46.4
B	6.8	22.9	-99.1	3.1	8.1	24.7	-4.8	21.8	-46.2	-1.8	17.6	-46.4
C	6.8	22.9	-99.1	3.1	8.1	24.7	-4.8	21.8	-46.2	-1.8	17.6	-46.4
D	6.8	22.9	-99.8	3.0	8.1	22.7	-4.9	21.7	-47.0	-1.8	17.5	-46.7
E	6.8	22.9	-99.5	3.0	8.2	24.3	-5.0	22.0	-46.3	-1.8	17.6	-47.3
F	6.8	22.9	-103.2	3.0	8.3	-23.0	-4.9	21.9	-54.5	-1.8	18.2	-47.6

TABLE 21. URES FOR DATA TYPES 0, 9, AND 4 (CM)

Case	Total		Orbit		Clock		Corr(R,C)
	RMS	Peak	RMS	Peak	RMS	Peak	
12	21.2	93.5	10.0	28.7	23.2	104.0	0.400
A	21.0	91.9	9.1	27.6	22.9	98.1	0.370
B	21.0	91.9	9.1	27.6	22.9	98.1	0.370
C	21.0	91.9	9.1	27.6	22.9	98.1	0.370
D	21.0	92.1	9.1	25.6	22.9	98.9	0.369
E	21.1	92.3	9.1	27.3	22.9	98.8	0.373
F	21.1	93.6	9.2	22.7	22.9	103.5	0.371

TABLE 22. GPS CLOCK AND ORBIT DIFFERENCES VS. "TRUTH" FOR DATA TYPES 0, 9, AND 5 (CM)

Case	Clock			Radial			Along-Track			Cross-Track		
	Mean	RMS	Peak	Mean	RMS	Peak	Mean	RMS	Peak	Mean	RMS	Peak
12	6.8	23.2	-105.4	3.2	8.8	25.8	-3.4	27.2	-60.7	-1.8	17.9	-45.1
A	7.2	21.4	-90.6	3.2	8.8	25.8	-3.4	27.2	60.7	-1.8	17.9	-45.1
B	10.2	23.3	-93.9	3.2	8.8	25.8	-3.4	27.2	60.7	-1.8	17.9	-45.1
C	12.0	27.7	-96.1	3.2	8.8	25.8	-3.4	27.2	60.7	-1.8	17.9	-45.1
D	7.2	21.2	-89.6	3.1	8.5	24.9	-3.8	26.8	59.3	-1.9	18.1	-44.3
E	9.4	24.3	-98.4	3.1	10.1	32.9	-3.9	31.7	64.6	-2.0	19.9	-49.0
F	10.1	27.8	-100.3	3.1	12.1	36.3	-3.3	33.2	68.7	-2.0	20.5	-50.6

TABLE 23. URES FOR DATA TYPES 0, 9, AND 5 (CM)

Case	Total		Orbit		Clock		Corr(R,C)
	RMS	Peak	RMS	Peak	RMS	Peak	
12	21.2	93.5	10.0	28.7	23.2	104.0	0.400
A	19.4	78.3	10.0	28.7	21.4	88.1	0.410
B	22.3	100.0	10.0	28.7	23.3	88.0	0.229
C	27.3	112.1	10.0	28.7	27.7	95.7	0.116
D	19.4	77.8	9.7	27.7	21.2	86.8	0.396
E	21.5	91.8	11.4	35.7	24.3	94.7	0.464
F	23.2	94.2	13.3	38.6	27.8	101.5	0.573

In the experiments with the treatment of the crosslink biases, the sensitivity of the statistical assumptions for the Gauss-Markov treatment of the crosslink biases was investigated. During these experiments, it was observed that as the *a priori* and steady-state sigmas were reduced below a critical threshold, not all of the introduced receiver biases could be absorbed by that parameter. This resulted in a departure, in a mean sense, between the estimated receiver bias parameter and the true receiver bias, with an increase in the departure as the statistics were further reduced. Recall that the receiver bias must be constrained for a single satellite. As a result, no receiver bias was introduced for this satellite. When estimating the transmitter-receiver biases, however, there was no requirement to constrain this parameter for a single satellite. The differences between the estimated transmitter-receiver bias and the true value, in a mean sense were zero over all satellites. For the satellite with the receiver bias constrained, it was noted that as the statistics were reduced, the increase in the difference between the estimated transmitter-receiver bias and the true value was nearly identically as the increase in the departure, in a mean sense, between the estimated receiver bias parameter and the true receiver bias for all of the other satellites. The transmitter-receiver bias for the constrained satellite was able to compensate for the decrease in the absorption of the receiver biases due to the reduction of the *a priori* and steady-state sigmas, while the other satellites adjusted to maintain an overall mean difference of approximately zero.

An additional sensitivity experiment was conducted with the treatment of the crosslink biases as a constant bias. This treatment was investigated to determine what would happen if periodic variations present within the crosslink biases were estimated with a model which did not allow for such variations. To gain this understanding, it was judged that sensitivity experiments with only data types 0, 9, and 3; and data types 0, 9, 4, and 5 needed to be conducted. For this experiment, treatments of the crosslink biases included unconstrained in the first-stage and as a constant in the second-stage filter, and as a constant in the first- and second-stage filters. Table 24 summarizes these sensitivity experiments. Orbit and clock differences from "truth" are presented in Tables 25 and 27 for types 0, 9, and 3 and types 0, 9, 4, and 5. The total, orbit, and clock UREs are presented in Tables 26 and 28 for types 0, 9, and 3 and types 0, 9, 4, and 5. Fits based on this treatment resulted in precise orbit and clock estimates which did not agree as well with "truth", because, as

expected, small amplitude sinusoidal crosslink bias variations present in the simulated data could not be properly accounted for.

TABLE 24. CONSTANT BIAS TREATMENT OF CROSSLINK BIASES AND STATISTICAL ASSUMPTIONS

Treatment of Crosslink Biases	Statistical Assumptions		Case
	First-stage filter	Second-stage filter	
Unconstrained in the first-stage filter, bias in the second-stage filter	AP = 0.1111×10^{-02} ns VR = 0.1111×10^{-02} ns^2/sec	AP = 5 ns	G
Bias in the first- and second stage filters	AP = 5 ns	AP = 5 ns	H

(AP = *A Priori*, VR = Variance Rate, SS = Steady-State Sigma, T = Tau)

TABLE 25. GPS CLOCK AND ORBIT DIFFERENCES VS. "TRUTH" FOR DATA TYPES 0, 9, AND 3 FOR CONSTANT BIAS EXPERIMENTS (CM)

Case	Clock			Radial			Along-Track			Cross-Track		
	Mean	RMS	Peak	Mean	RMS	Peak	Mean	RMS	Peak	Mean	RMS	Peak
12	6.8	23.2	-105.4	3.2	8.8	25.8	-3.4	27.2	-60.7	-1.8	17.9	-45.1
G	7.8	23.0	-95.0	3.1	8.1	24.8	-4.8	21.8	-46.8	-1.8	17.6	-46.4
H	7.7	23.0	-97.1	3.0	7.9	21.7	-4.9	21.0	55.4	-1.8	17.9	-46.4

TABLE 26. URES FOR DATA TYPES 0, 9, AND 3 FOR CONSTANT BIAS EXPERIMENTS (CM)

Case	Total		Orbit		Clock		Corr(R,C)
	RMS	Peak	RMS	Peak	RMS	Peak	
12	21.2	93.5	10.0	28.7	23.2	104.0	0.400
G	21.4	87.0	9.1	27.7	23.0	97.1	0.330
H	21.3	86.8	8.8	25.1	23.0	99.1	0.332

TABLE 27. GPS CLOCK AND ORBIT DIFFERENCES VS. "TRUTH" FOR DATA TYPES 0, 9, 4, AND 5 FOR CONSTANT BIAS EXPERIMENTS (CM)

Case	Clock			Radial			Along-track			Cross-track		
	Mean	RMS	Peak	Mean	RMS	Peak	Mean	RMS	Peak	Mean	RMS	Peak
12	6.8	23.2	-105.4	3.2	8.8	25.8	-3.4	27.2	-60.7	-1.8	17.9	-45.1
G	12.9	26.9	-95.9	3.1	8.1	24.7	-4.8	21.8	-46.2	-1.8	17.6	-46.4
H	10.6	26.0	-97.6	3.0	11.3	32.6	-5.4	27.0	67.5	-1.8	19.6	-46.7

TABLE 28. URES FOR DATA TYPES 0, 9, 4, AND 5 FOR CONSTANT BIAS EXPERIMENTS (CM)

Case	Total		Orbit		Clock		Corr(R,C)
	RMS	Peak	RMS	Peak	RMS	Peak	
12	21.2	93.5	10.0	28.7	23.2	104.0	0.400
G	26.5	104.5	9.1	27.6	26.9	102.4	0.064
H	20.7	90.0	12.2	35.4	26.0	97.7	0.649

Sensitivity Analysis

Additional experiments were conducted to determine the sensitivity of the orbit and clock estimates to various processing scenarios. As with the previous experiments, 3-day fits were performed for the first day, with the middle day of the fit used to determine relative GPS orbit and clock accuracy and to quantify the effects of the various experiments. For simplicity of reporting results, all additional sensitivity experiments conducted treated the crosslink biases as Gauss-Markov processes in the first- and second-stage filters. The experiments with data types 0, 9, and 3, data types 0, 9, and 4, and data types 0, 9, and 5 used *a priori* and steady-state sigmas of 5 ns. The experiments with data types 0, 9, 4, and 5 used an *a priori* sigma of 5 ns and a steady-state sigma of 0.75 ns. Again, for simplicity of reporting results, each combination of data types used in the additional sensitivity experiments will be assigned a case number. Fits based on data types 0, 9, and 3 will be referred to as Case 1, fits based on data types 0, 9, 4, and 5 will be referred to as Case 2, fits based on data types 0, 9, and 4 will be referred to as Case 3, and fits based on data types 0, 9, and 5 will be referred to as Case 4. Orbit and clock estimates derived from the additional sensitivity experiments that follow will be compared with the orbit and clock estimates from these selected cases. Orbit and clock differences from "truth" for these selected cases are presented in Table 29. The total, orbit, and clock UREs for these selected cases are presented in Table 30 and summarized in Figure 4.

TABLE 29. GPS CLOCK AND ORBIT DIFFERENCES VS. "TRUTH" FOR SELECTED CASES (CM)

Case	Clock			Radial			Along-Track			Cross-Track		
	Mean	RMS	Peak	Mean	RMS	Peak	Mean	RMS	Peak	Mean	RMS	Peak
1	6.8	22.8	-99.3	3.0	8.1	22.5	-5.0	21.6	-46.3	-1.8	17.6	-47.4
2	7.8	20.2	-86.3	3.0	7.9	23.1	-5.7	21.7	57.1	-1.8	18.6	-48.6
3	6.8	22.9	-99.8	3.0	8.1	22.7	-4.9	21.7	-47.0	-1.8	17.5	-46.7
4	7.2	21.2	-89.6	3.1	8.5	24.9	-3.8	26.8	59.3	-1.9	18.1	-44.3

TABLE 30. URES FOR SELECTED CASES (CM)

Case	Total		Orbit		Clock		Corr(R,C)
	RMS	Peak	RMS	Peak	RMS	Peak	
1	21.0	91.1	9.0	25.3	22.8	98.6	0.364
2	18.4	81.7	8.9	26.1	20.2	85.0	0.373
3	21.0	92.1	9.1	25.6	22.9	98.9	0.369
4	19.4	77.8	9.7	27.7	21.2	86.8	0.396

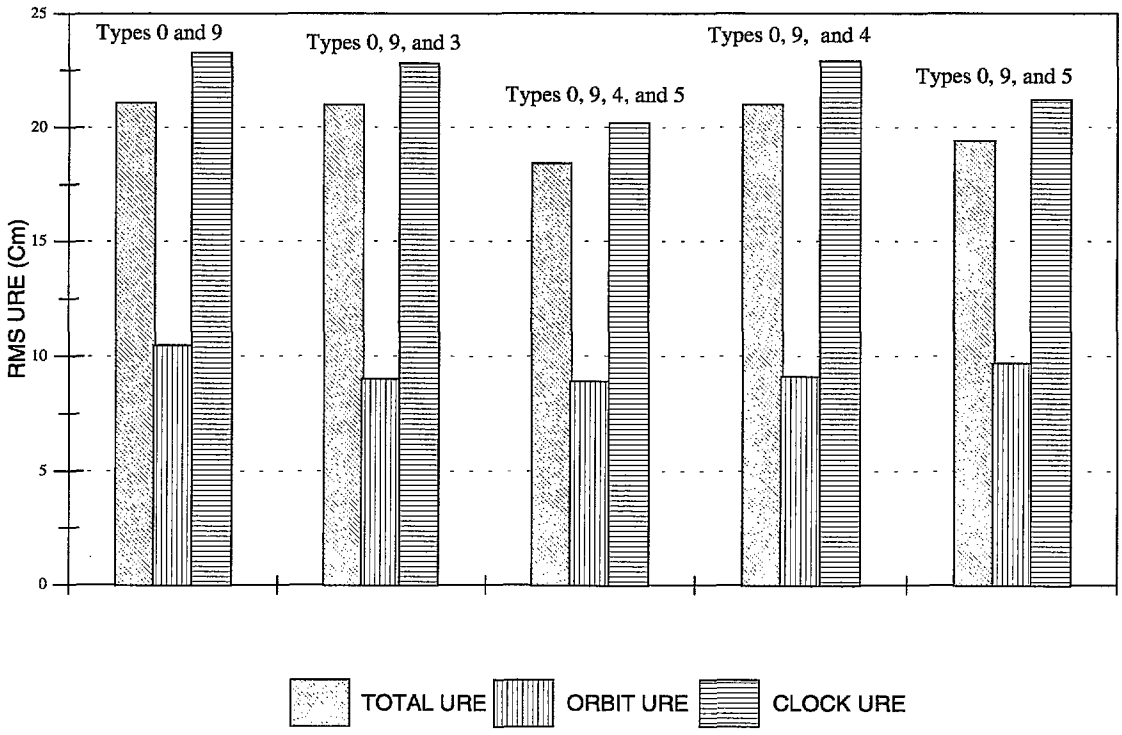

FIGURE 4. RMS URES FOR DATA TYPE COMBINATIONS

An experiment was conducted to determine the sensitivity of the orbit and clock estimates to the treatment of the phasing of the crosslink transmitter and receiver biases for each satellite. The phasing is one aspect of the crosslink biases and is implemented through the simulator. For the experiments presented thus far, the phasing was treated as random. With the treatment of the phasing as common, for a particular satellite, the transmitter and receiver have identical phasing. This phasing was unique for each satellite. Orbit and clock differences from "truth" are presented in Table 31 and the total, orbit, and clock UREs are presented in Table 32. Insignificant differences were seen in the orbit and clock estimates for Case 1, whereas orbit and clock estimates for Case 2 were slightly degraded.

TABLE 31. GPS CLOCK AND ORBIT DIFFERENCES VS. "TRUTH" FOR PHASING SENSITIVITY EXPERIMENTS (CM)

Case	Clock			Radial			Along-track			Cross-track		
	Mean	RMS	Peak	Mean	RMS	Peak	Mean	RMS	Peak	Mean	RMS	Peak
1	6.8	22.8	-99.2	3.0	8.1	23.1	-5.1	21.6	-46.4	-1.8	17.6	-47.3
2	7.9	20.9	-87.7	3.0	8.4	23.0	-5.8	22.6	58.2	-1.8	18.7	-48.2

TABLE 32. URES FOR PHASING SENSITIVITY EXPERIMENTS (CM)

Case	Total		Orbit		Clock		Corr(R,C)
	RMS	Peak	RMS	Peak	RMS	Peak	
1	21.0	91.4	9.0	26.0	22.8	98.5	0.365
2	18.6	82.7	9.4	26.1	20.9	85.7	0.431

An experiment was conducted to determine the sensitivity of the orbit and clock estimates to a reduction in the measurement noise on the crosslink data. The single-frequency pseudorange noise introduced through the simulator was reduced 50%, from 33 cm to 16.5 cm. The observations sigmas used in the filter were also reduced accordingly. Orbit and clock differences from "truth" are presented in Table 33 and the total, orbit, and clock UREs are presented in Table 34. Insignificant differences in the overall accuracy were seen. Small improvements were noted in the orbit estimates, primarily in the along-track direction, for Cases 1, 2, and 3. However, these improvements were largely offset by a decrease in the correlation between the orbit radial direction and clock component for these data combinations. No change in orbit and clock estimates were noted for Case 4.

TABLE 33. GPS CLOCK AND ORBIT DIFFERENCES VS "TRUTH" FOR REDUCTION IN NOISE SENSITIVITY EXPERIMENTS (CM)

Case	Clock			Radial			Along-Track			Cross-Track		
	Mean	RMS	Peak	Mean	RMS	Peak	Mean	RMS	Peak	Mean	RMS	Peak
1	6.7	22.2	-93.0	2.9	7.1	18.7	-7.6	18.1	37.9	-1.7	16.6	-43.0
2	7.9	20.1	-83.5	2.9	7.4	-19.8	-8.4	19.6	45.1	-1.8	18.2	-47.6
3	6.6	22.4	-94.0	2.9	7.2	18.8	-7.5	18.1	37.5	-1.8	16.6	-42.4
4	7.1	21.1	-88.7	3.1	8.5	24.9	-3.9	26.8	59.2	-1.9	18.1	-44.2

TABLE 34. URES FOR REDUCTION IN NOISE SENSITIVITY EXPERIMENTS (CM)

Case	Total		Orbit		Clock		Corr(R,C)
	RMS	Peak	RMS	Peak	RMS	Peak	
1	20.7	90.2	8.0	21.6	22.2	92.3	0.313
2	18.4	82.6	8.4	22.3	20.1	85.6	0.352
3	20.9	91.7	8.0	21.7	22.4	93.3	0.318
4	19.2	77.0	9.7	27.7	21.1	85.9	0.399

Experiments were conducted to determine the sensitivity of the orbit and clock estimates to a reduction in the number of stations. These experiments were designed to evaluate if inclusion of the crosslink data would offset the reduction in station tracking data and maintain orbit and clock quality. Both the 7-station NIMA network and OCS station network were used in this evaluation. Figure 5 gives the 7-station NIMA network and Figure 6 gives the 5-station OCS network. For the OCS network, Colorado Springs was selected as the master station.

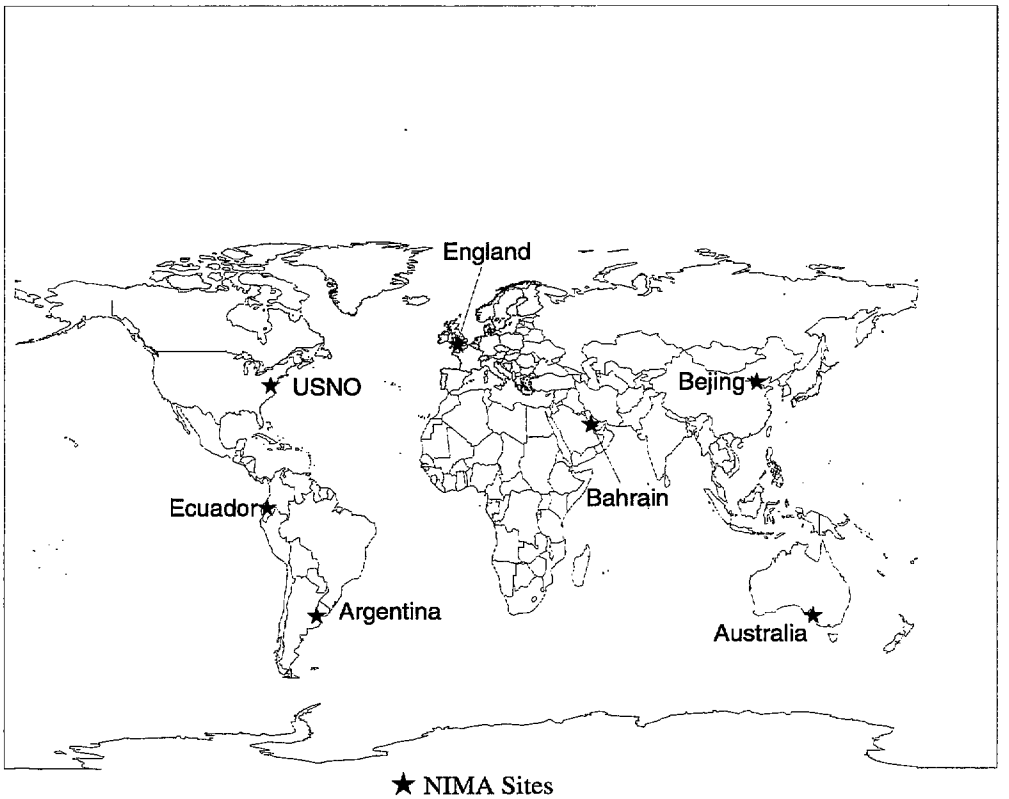

★ NIMA Sites

FIGURE 5. 7-STATION NIMA NETWORK

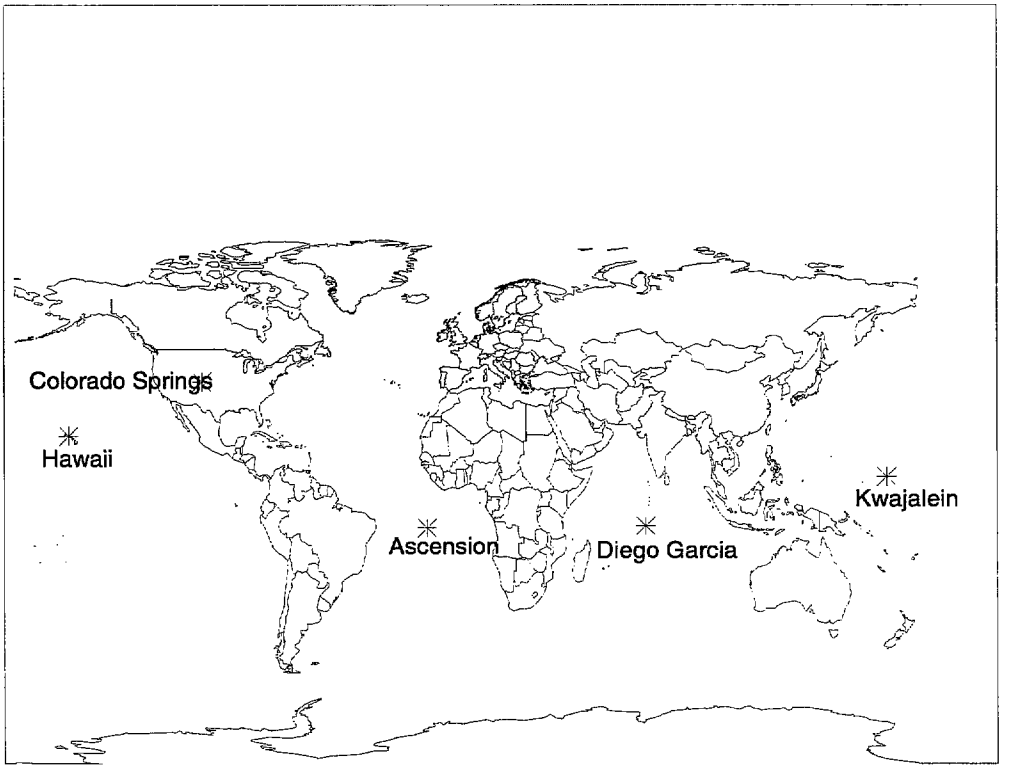

✳ Air Force Sites

FIGURE 6. 5-STATION OCS NETWORK

Using station-tracking pseudorange and range difference observations from the NIMA sites only, as compared to the selected cases reported in Tables 29 and 30, resulted in significantly degraded orbit and clock estimates for each combination of data types. Orbit and clock differences from "truth" are presented in Table 35 and the total, orbit, and clock UREs are presented in Table 36. Among the orbit components, the along-track mean differences experienced the worst degradation with respect to "truth", with a significant bias present for all cases. The bias ranged from -10.9 cm for Case 4 to -15.6 cm for Case 2 as compared to a range of -3.8 cm to -5.7 cm for the selected cases. The along-track RMS differences ranged from 28.9 cm for Case 1 to 35.5 cm for Case 4 as compared to 21.6 cm to 26.8 cm for the selected cases. The degradation in the other orbit components was less apparent, with no appreciable change in the mean differences. The largest degradation in the RMS differences occurred with Case 4, which changed from 8.5 cm to 11.5 cm in the radial component, and from 18.1 cm to 30.6 cm in the cross-track component. The degradation of the clock components was not as significant as compared to the degradation of the orbit components. The largest degradation occurred for Case 4, where the mean differences changed from 7.2 cm to 9.1 cm. Essentially no change occurred for Case 2. The small degradation in the clocks as well as an increase in the correlation between the radial orbit differences and the clock differences resulted in the total, orbit, and clock UREs for Case 2 that were still comparable to the 12-station baseline case. The total URE for this case was 20.9 cm as compared to 21.1 cm for the 12-station baseline case.

TABLE 35. GPS CLOCK AND ORBIT DIFFERENCES VS. "TRUTH" FOR REDUCTION IN STATIONS, NIMA SITES ONLY (CM)

Case	Clock			Radial			Along-Track			Cross-Track		
	Mean	RMS	Peak	Mean	RMS	Peak	Mean	RMS	Peak	Mean	RMS	Peak
1	7.7	26.2	-109.2	2.9	9.0	-27.0	-14.1	28.9	60.2	-1.8	26.1	-86.8
2	7.9	22.7	94.0	2.8	10.2	-28.2	-15.6	32.2	-71.4	-1.8	28.8	-94.9
3	7.8	26.5	-110.0	2.9	9.1	-27.1	-13.6	29.0	60.2	-1.8	25.7	-83.0
4	9.1	24.8	-92.2	3.3	11.5	32.7	-10.9	35.5	113.2	-2.0	30.6	-115.4

TABLE 36. URES FOR REDUCTION IN STATIONS, NIMA SITES ONLY (CM)

Case	Total		Orbit		Clock		Corr(R,C)
	RMS	Peak	RMS	Peak	RMS	Peak	
1	25.0	111.9	10.6	29.5	26.2	113.4	0.305
2	20.9	105.6	11.9	28.4	22.7	103.6	0.420
3	25.1	110.3	10.7	30.0	26.5	114.9	0.315
4	22.4	104.0	13.3	37.6	24.8	99.8	0.449

Using station-tracking pseudorange and range difference observations from the OCS sites only, as compared to the selected cases reported in Tables 29 and 30, again resulted in significantly degraded orbits and clock for all crosslink data combinations. Orbit and clock differences from "truth" are presented in Table 37 and the total, orbit, and clock UREs are presented in Table 38. Generally, the amount of degradation with respect to "truth" was larger for each component as compared to the experiments with the NIMA sites. In particular, the degradation in the orbit components for Case 4 was most apparent, with a change in the RMS differences from 11.5 cm to 15.9 cm in the radial direction, from 35.5 cm to 64.2 cm in the along-track component and from 30.6 cm to 50.5 cm in the cross-track component. The mean difference in the along-track component degraded from -10.9 cm to -24.4 cm. For the other cases, the most significant degradation in the RMS differences occurred in the along-track direction. The clock mean differences with respect to "truth" actually improved for all data combinations as compared to the experiments with the NIMA sites. The largest improvement occurred with Case 4, with a change from 9.1 cm to 1.3 cm. The clock RMS differences with respect to "truth", however, degraded 4 or 5 cm for each case as compared to the experiments with the NIMA sites, except for Case 2, which improved by 0.8 cm.

The overall URE degraded for all of the cases as compared to the experiments with the NIMA sites. The cases which included the derived clock observations (type 5) however, did not degrade as significantly, with Case 2 remaining essentially the same. For these fits, the degradation in the orbit components is compensated by the improvement in the clock contribution and resulted in the total, orbit, and clock UREs for fits derived for Case 2 that were still comparable to the 12-station baseline case. The total URE for this case was 21.0 cm as compared to the total URE of 21.1 cm for the 12-station baseline case. This may be attributed to the improved geographic distribution of the OCS sites, although there are 2 less stations as compared to the NIMA network.

TABLE 37. GPS CLOCK AND ORBIT DIFFERENCES VS. "TRUTH" FOR REDUCTION IN STATIONS, OCS SITES ONLY (CM)

Case	Clock			Radial			Along-Track			Cross-Track		
	Mean	RMS	Peak	Mean	RMS	Peak	Mean	RMS	Peak	Mean	RMS	Peak
1	-3.7	30.0	-135.2	2.9	11.7	34.5	-14.0	38.7	90.4	-1.8	24.8	63.9
2	1.2	21.9	-95.2	2.9	11.7	-35.3	-17.6	38.3	81.9	-1.6	25.1	71.3
3	-4.8	32.2	-144.4	2.9	12.0	35.6	-12.7	39.1	93.5	-1.9	25.6	67.2
4	1.3	29.0	-102.4	4.3	15.9	40.8	-24.4	64.2	-186.6	-1.7	50.5	159.6

TABLE 38. URES FOR REDUCTION IN STATIONS, OCS SITES ONLY (CM)

Case	Total		Orbit		Clock		Corr(R,C)
	RMS	Peak	RMS	Peak	RMS	Peak	
1	29.3	124.8	13.4	39.7	30.0	133.1	0.355
2	21.0	98.7	13.4	35.1	21.9	98.2	0.428
3	31.2	149.2	13.8	40.7	32.2	147.3	0.381
4	26.8	96.7	19.7	48.4	29.0	117.1	0.564

Using the station tracking pseudorange and range difference observations from the NIMA sites only, an experiment was conducted where the measurement noise on the crosslink data was reduced by 50%. These experiments were designed to evaluate if this reduction in the measurement noise would offset the degradation of the orbit and clock estimates due to the reduced station network. Orbit and clock differences from "truth" are presented in Table 39 and the total, orbit, and clock UREs are presented in Table 40. When using the reduced measurement noise on the crosslink data with the NIMA stations only, insignificant differences in the overall accuracy were seen. Fits based on using the derived clock observations (type 5) experienced the smallest improvements as compared to the experiments with the NIMA sites only. Case 4 demonstrated no appreciable change. With the other data combinations, small improvements were seen in the orbit and clock components, but the correlation between the radial orbit differences and the clock differences decreased. This resulted in only small improvements in the total UREs.

TABLE 39. GPS CLOCK AND ORBIT DIFFERENCES VS. "TRUTH" FOR REDUCTION IN NOISE SENSITIVITY EXPERIMENTS, NIMA SITES ONLY (CM)

Case	Clock			Radial			Along-Track			Cross-Track		
	Mean	RMS	Peak	Mean	RMS	Peak	Mean	RMS	Peak	Mean	RMS	Peak
1	7.1	24.9	-108.9	2.9	7.3	-20.9	-16.9	25.3	54.3	-1.8	24.1	-64.0
2	7.9	22.2	92.7	2.8	8.9	-25.6	-18.5	29.4	-57.1	-1.8	27.2	75.9
3	7.2	25.6	-107.8	2.9	7.4	-20.8	-16.5	25.2	54.7	-1.8	23.9	-61.3
4	9.1	24.6	90.8	3.3	11.5	32.7	-10.9	35.5	112.2	-2.0	30.5	-115.1

TABLE 40. URES FOR REDUCTION IN NOISE SENSITIVITY EXPERIMENTS, NIMA SITES ONLY (CM)

Case	Total		Orbit		Clock		Corr(R,C)
	RMS	Peak	RMS	Peak	RMS	Peak	
1	24.1	112.2	8.8	22.2	24.9	113.5	0.235
2	20.8	101.7	10.6	28.1	22.2	102.2	0.368
3	24.7	111.4	8.9	22.5	25.6	116.9	0.246
4	22.3	103.8	13.3	37.6	24.6	99.1	0.452

Figure 7 summarizes the total, orbit, and clock UREs for each of the sensitivity experiments for Case 2 (data types 0, 9, 4, and 5). This data combination consistently proved to produce superior orbit and clock estimates as compared to the other data combinations. Comparison of the experiments reveal little sensitivity to the treatment of the phasing of the transmitter and receiver for each satellite as well as the noise levels of the crosslink data. The reduced station network experiments resulted in similarly degraded orbit and clock estimates for both the NIMA and OCS networks. Reducing the measurement noise with the NIMA network again revealed little sensitivity.

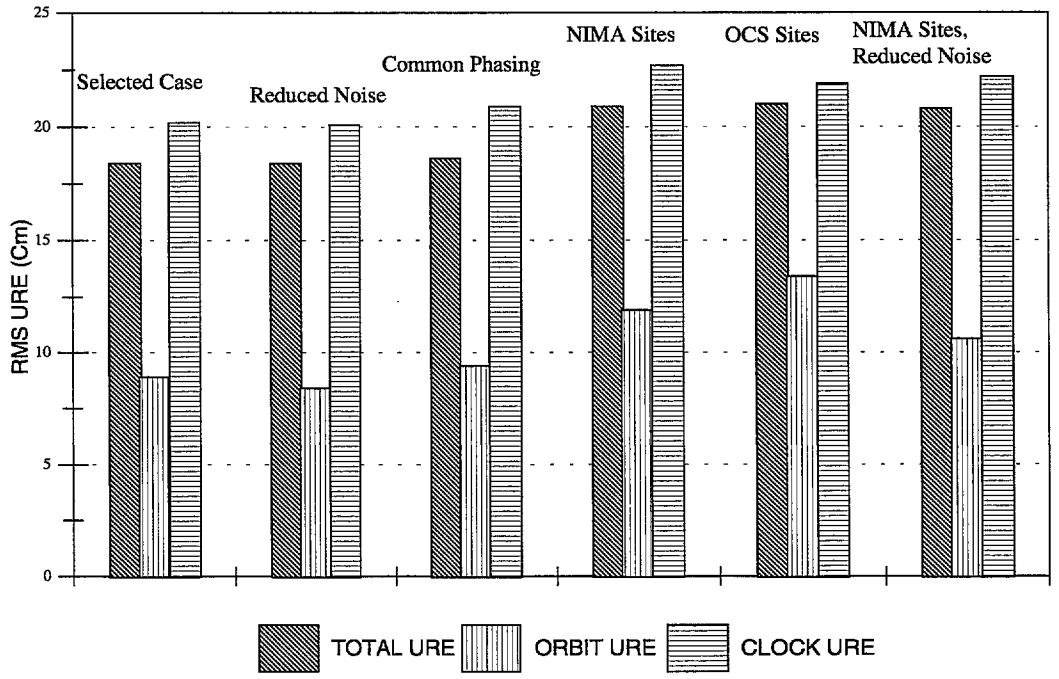

FIGURE 7. RMS URES FOR DATA TYPES 0, 9, 4, AND 5 FOR SENSITIVITY ANALYSIS CASES

The Earth orientation estimates generated for each of the 3 three-day fit spans for data types 0, 9, 4, and 5 were compared with estimates generated for the 12-station baseline case. These comparisons are given in Table 41. Only values at the beginning and end of each day are given. For the 3 days of interest the differences in x and y correspond to about 3 millimeters and the differences in UT1-UTC correspond to about 5 millimeters at the Earth's surface. These extremely small differences indicate that the Earth orientation estimates are consistent for both fits. This result corroborates that, as the crosslink data has no direct link to the ground, there is no information content related to Earth orientation.

TABLE 41. COMPARISON OF EARTH ORIENTATION ESTIMATES

Fit Day #	Day #	Data Types	x(")	y(")	UT1-UTC(s)
321	321	0 and 9	-0.0473	0.4395	0.30189
		0, 9, 4, and 5	-0.0474	0.4396	0.30188
	322	0 and 9	-0.0469	0.4402	0.29959
		0, 9, 4, and 5	-0.0469	0.4403	0.29958
322	322	0 and 9	-0.0468	0.4404	0.29933
		0, 9, 4, and 5	-0.0468	0.4405	0.29934
	323	0 and 9	-0.0464	0.4416	0.29699
		0, 9, 4, and 5	-0.0463	0.4416	0.29700
323	323	0 and 9	-0.0463	0.4416	0.29674
		0, 9, 4, and 5	-0.0463	0.4417	0.29674
	324	0 and 9	-0.0458	0.4427	0.29434
		0, 9, 4, and 5	-0.0458	0.4427	0.29434

Evaluation of Orbit and Clock Accuracy

The sensitivity experiments discussed above have provided a more complete understanding of the characteristics and relative information content of the crosslink ranging data types. To determine the overall achievable orbit and clock accuracy through incorporating the crosslink data with station data, fits based on the selected cases were performed for two additional days and used to form overall statistics. These are compared with the equivalent fits from the 12-station baseline case and 18-station future case.

Figure 8 compares the overall total, orbit, and clock RMS UREs for each of the selected cases with the 12- and 18-station network cases. Orbit and clock estimates based on data types 0, 9, 4, and 5 together resulted in the largest improvement as compared with the 12-station baseline case. The improvement in the clock estimates were the most apparent, with the clock URE

improving from 23.3 cm to 20.2 cm. Clock estimates based on data types 0, 9, and 5 also improved slightly as compared with the 12-station baseline case. The improvement in the clock estimates for these two cases is attributable to the low noise level associated with the derived clock data. The improvement in the orbit estimates derived for each of the selected cases was very small as compared with the 12-station baseline case. Orbit and clock estimates based on data types 0, 9, and 4 did not result in any appreciable improvement.

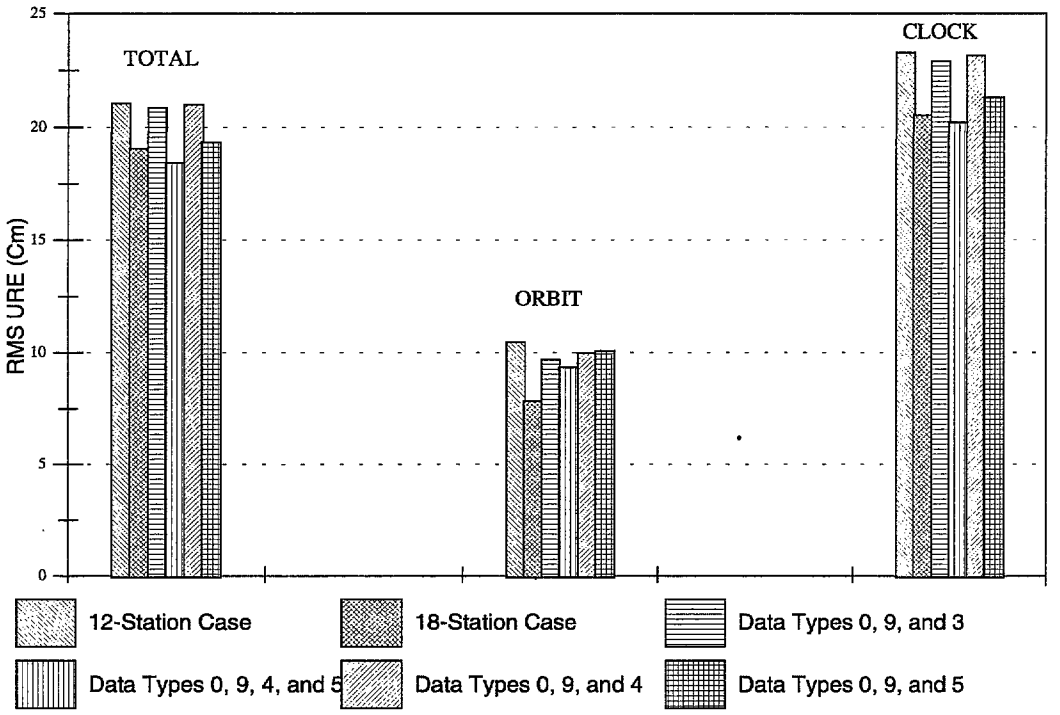

FIGURE 8. RMS URES FOR SELECTED CASES AND STATION-ONLY CASES

Only the fits based on data types 0, 9, 4, and 5 together demonstrated accuracy comparable with the 18-station future case. The clock estimates for this case were slightly better, whereas the orbit estimates were not as accurate. There was an increase in the correlation between the radial orbit differences and the clock differences, as the overall total URE for orbit and clock estimates based on data types 0, 9, 4, and 5 together were slightly better than for the 18-station future case.

Figure 9 compares overall total, orbit, and clock RMS UREs for the reduced station network experiments for data types 0, 9, 4, and 5 with the 12-station baseline case. Fits based on data types 0, 9, 4, and 5 with the NIMA sites only demonstrated accuracy comparable with the 12-station network. Again, the clock estimates for this case were slightly better, whereas the orbit estimates were not as accurate. An increase in the correlation between the radial orbit differences and the clock differences accounted for the improvement in the total URE. Orbit and clock estimates based on data types 0, 9, 4, and 5 with the OCS sites only were not as good.

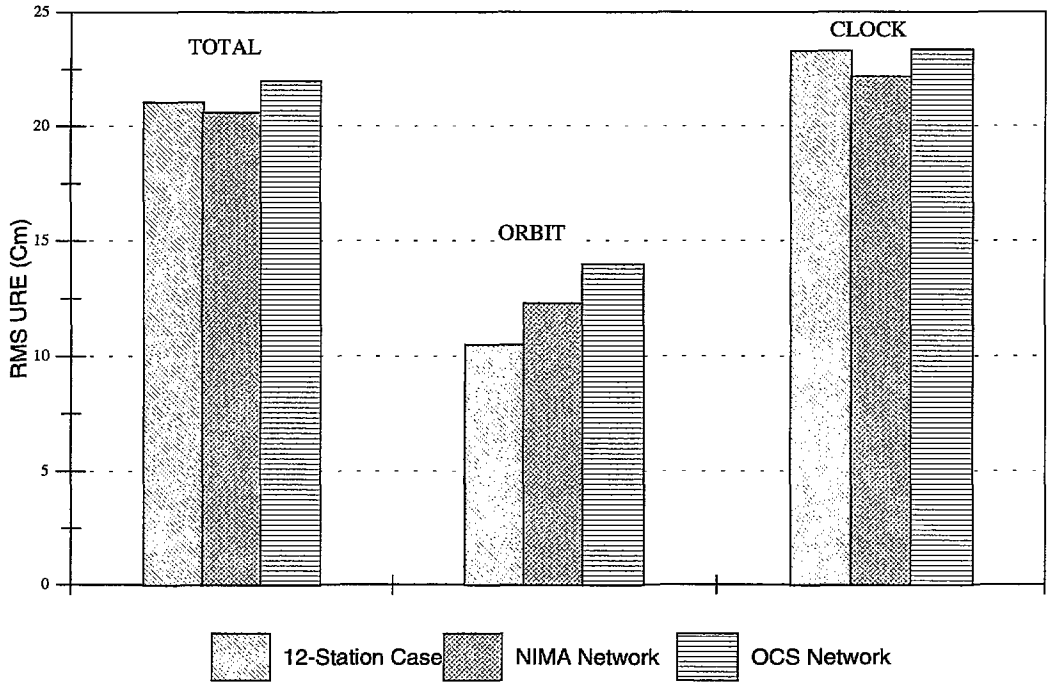

FIGURE 9. RMS URES FOR DATA TYPES 0, 9, 4, AND 5
FOR REDUCED STATION NETWORKS

Figure 10 compares overall total, orbit, and clock RMS UREs from an experiment using crosslink data with the 18-station network with the 18-station future case. Again, orbit and clock estimates based on data types 0, 9, 4, and 5 together resulted in the largest improvement as compared to the 18-station future case. The improvement in the clock estimates was the most apparent, with the clock URE improving from 20.5 to 18.8 cm. An improvement in the clock estimates based on data types 0, 9, and 5 was also attributable to the low noise level associated with the derived clock data. The improvement in the orbit estimates derived for each of the selected cases was very small as compared with the 18-station future case.

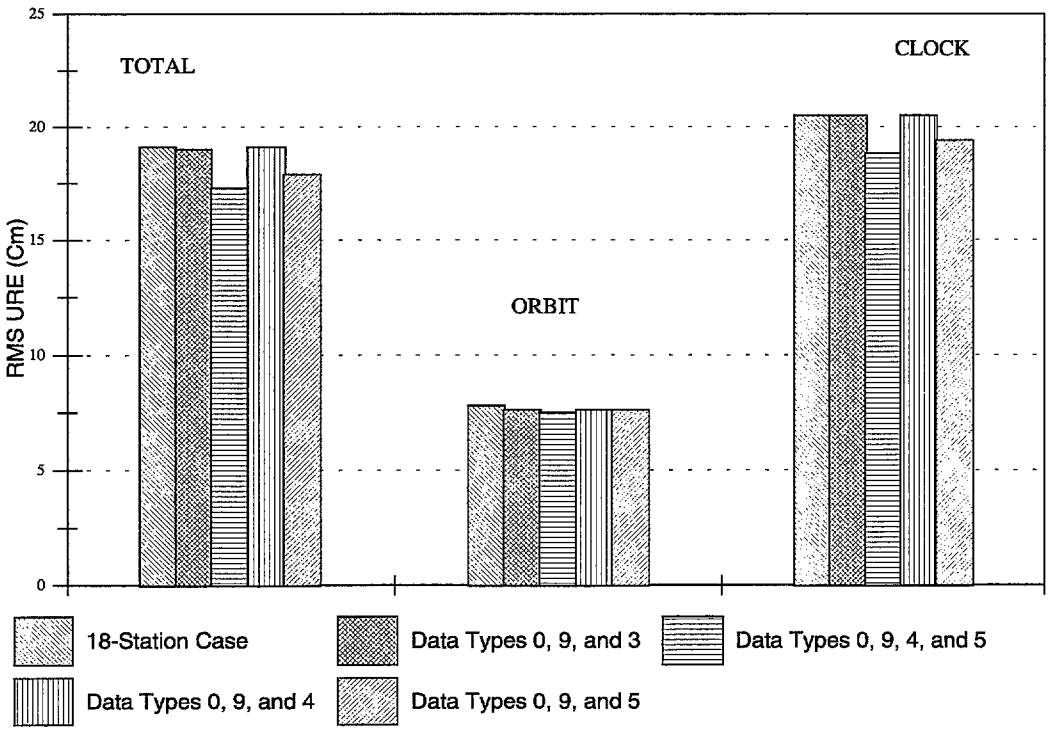

FIGURE 10. RMS URES FOR USING CROSSLINK DATA WITH 18-STATIONS AND 18-STATION FUTURE CASE

The sensitivity of the orbit and clock estimates to the presence and assumptions for estimating the crosslink biases was also investigated. Four sets of orbit and clock estimates were generated and compared for the purpose of determining the sensitivity to the inclusion and estimation of the crosslink biases. Three-day fits were performed using station-tracking pseudorange and range difference data from the 12-station network with crosslink derived distance and clock data (types 0, 9, 4, and 5). Case 2 was chosen to be the selected case as described previously, with the crosslink biases treated as Gauss-Markov processes in the first- and second-stage filters, with an *a Priori* of 5 ns, steady-state sigma of 0.75 ns, and tau of 4 hours. For the remaining three cases, no crosslink biases were introduced into the observations through the data simulator. For cases 2a and 2b, however, crosslink biases were estimated. With case 2a, the crosslink biases were again treated as Gauss-Markov processes, with the same statistics as case 1. With case 2b, the crosslink biases were treated as biases, with an *a Priori* of 5 ns. Crosslink biases were not estimated for case 2c.

Figure 11 compares overall total, orbit, and clock RMS UREs for each of these cases for three 3-day fits. The statistics are reported for the middle day of each fit. As the improvement in the total URE is small, these results indicate that the crosslink biases are being accommodated in the estimation process, and there is little penalty for estimating this parameter even when there is no introduced error. Comparison of case 2 with case 2c provides a direct measure of how well the crosslink biases are being estimated. The level of agreement between the total URE for these two cases remains good as a result of the increase in the correlation between the orbit and clock estimates for case 2, when crosslink biases are both present and estimated. Orbit and clock estimates, individually, do improve significantly when crosslink biases are not present and estimated.

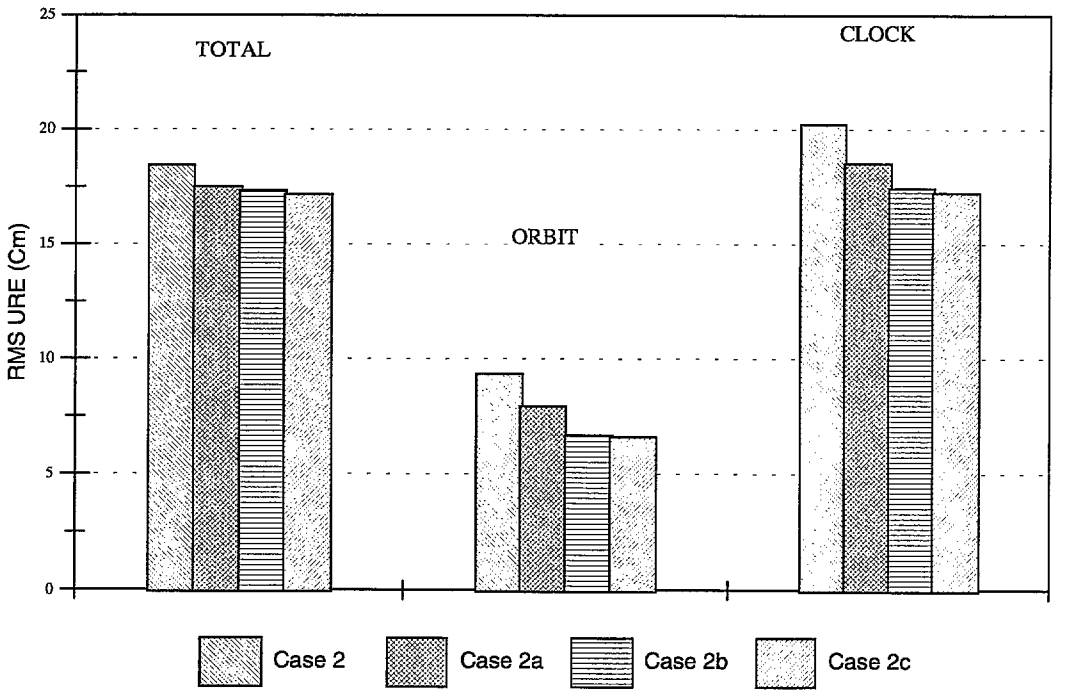

FIGURE 11. SENSITIVITY OF ORBIT AND CLOCK ESTIMATES TO THE INCLUSION AND ESTIMATION OF CROSSLINK BIASES

The total UREs for cases 2a and 2b are nearly identical with case 2c, indicating little sensitivity to the quality of orbit and clock estimates to estimating crosslink biases which are not present. Direct comparisons of case 2a with case 2c indicate a small degradation in orbit and clock estimates due to the Gauss-Markov treatment, but an increase in the correlation between the orbit and clock estimates for case 2a compensates for these differences. Direct comparisons of case 2b with case 2c indicate near identical agreement in orbit and clock estimates with the treatment as a bias.

SUMMARY AND CONCLUSIONS

Much insight has been gained, through data simulations, of the characteristics and relative information content of the crosslink data types. Initially, a series of 3-day fits were performed to determine relative GPS orbit and clock accuracy based on different treatments of the crosslink biases and various assumed statistics for each of the data combinations. These experiments revealed that treatment of the crosslink biases as Gauss-Markov processes in the first- and second-stage filters consistently produced orbit and clock estimates with the best agreement with "truth". The best results for the fits based on data types 0, 9, and 3, data types 0, 9, and 4, and data types 0, 9, and 5 used *a priori* and steady-state sigmas of 5 ns and fits based on data types 0, 9, 4, and 5 used an *a priori* sigma of 5 ns and a steady-state sigma of 0.75 ns.

Additional experiments were conducted to determine the sensitivity of precise orbit and clock estimates to various processing scenarios, including the treatment of the phasing of the transmitter and receiver periodics, the reduction in the number of stations, and the reduction in the crosslink measurement noise. Comparison of the experiments revealed little sensitivity to the treatment of the phasing as random as compared to common as well as to the noise level of the crosslink data. The reduced station network experiments resulted in similarly degraded orbit and clock estimates for both the NIMA and OCS networks. Reducing the measurement noise with the NIMA network again revealed little sensitivity. Figure 5 summarized the total UREs for each of the sensitivity experiments for data types 0, 9, 4, and 5.

The overall achievable orbit and clock accuracy through incorporating the crosslink data with station tracking data is reported in Table 42. Using 5 days of data, precise orbit and clock estimates were generated for 3 three-day fit spans for the selected case for each combination of data types. Analysis revealed that fits based on data types 0, 9, 4, and 5 consistently produced superior orbit and clock estimates as compared to the other data combinations. Fits based on data types 0, 9, 4, and 5 together result in the largest improvement as compared with the 12-station baseline case and demonstrate accuracy comparable with the 18-station future case. The overall total URE for orbit and clock estimates based on data types 0, 9, 4, and 5 was 18.4 cm as compared to 19.1 cm for the 18-station future case. Figure 6 summarized the overall total, orbit, and clock UREs for the selected case for data types 0, 9, 4, and 5 and both the 12-station baseline and 18-station future networks. Fits based on data types 0, 9, 4, and 5 with the NIMA sites only demonstrated accuracy comparable with the 12-station baseline case. The overall total URE for orbit and clock estimates based on data types 0, 9, 4, and 5 with the NIMA sites only was 20.6 cm as compared to 21.1 cm for the 12-station baseline case. Figure 7 compared overall total, orbit, and clock RMS UREs for the reduced station network experiments for data types 0, 9, 4, and 5 with the 12-station baseline network.

TABLE 42. EXPECTED IMPROVEMENT IN URES WITH THE INCLUSION OF CROSSLINK RANGING DATA

Network Size	Data Types	Total	Orbit	Clock
12-Station	0 and 9	21.1	10.5	23.3
	0, 9, 4, and 5	18.4	9.3	20.2
18-Station	0 and 9	19.1	7.8	20.5
	0, 9, 4, and 5	17.3	7.5	18.8

These results indicate that the inclusion of the crosslink data with station data is equivalent to the inclusion of additional stations. In particular, the low noise levels associated with the derived clock observations will improve the quality of the precise clock estimates. The crosslink data could be used to improve the total URE to be comparable with the 18-station future network. As NIMA adds future tracking sites, the inclusion of the crosslink data will further improve the quality of the precise clock estimates. Because these results are based on simulations, it is evident that as the crosslink data become available in the future, additional studies using these data should be conducted to independently evaluate and verify the quality of the orbit and clock estimates.

REFERENCES

1. Swift, E. R., *Crosslink Ranging Formulation For OMNIS*, Dec 1995.

2. Fliegel, H. F., Gallini, T. E., and Swift, E. R., *Global Positioning System Radiation Force Model for Geodetic Applications*, Journal of Geophysical Research, Vol. 97, No. B1, Pages 559-568, Jan 10, 1992.

3. Herman, Bruce R., *Allan Variance Model Parameters Determined from OMNIS Satellite Clock Files*, Study Report to NIMA, Mar 1994.

4. Cunningham, J. P., *Improving the NIMA Precise GPS Orbit and Clock Estimates Through OMNIS Filter/Smoother Retuning*, Study Report to NIMA, Jun 1997.

5. Cunningham, J. P., and Swift, E. R., *Additional DMA Tracking Sites For Improving GPS Orbit and Clock Estimates,* NSWCDD/TR-95/70, Dahlgren, VA, Jun 1995.

6. Doyle, Larry, *Potential Autonav Accuracy Improvement,* GPS Control Segment Performance and Analysis Working Group Meeting, Falcon Air Force Base, Aug 1996.

7. Ananda, M. P., Bernstein, H., Cunningham, K. E., Feess, W. A., and Stroud, E. G., *Global Positioning System (GPS) Autonomous Navigation,* IEEE Plans, Mar 1990.


NAVSEA
DAHLGREN